Drychampones A–C: Three Meroterpenoids from *Dryopteris championii*

Neng-Hua Chen,[§] Yu-Bo Zhang,[§] Xiao-Jun Huang, Lin Jiang, Si-Qi Jiang, Guo-Qiang Li, Yao-Lan Li,[*] Guo-Cai Wang[*]

Institute of Traditional Chinese Medicine & Natural Products, College of Pharmacy, Jinan University, Guangzhou 510632, People's Republic of China

Supporting Information Placeholder

Contents

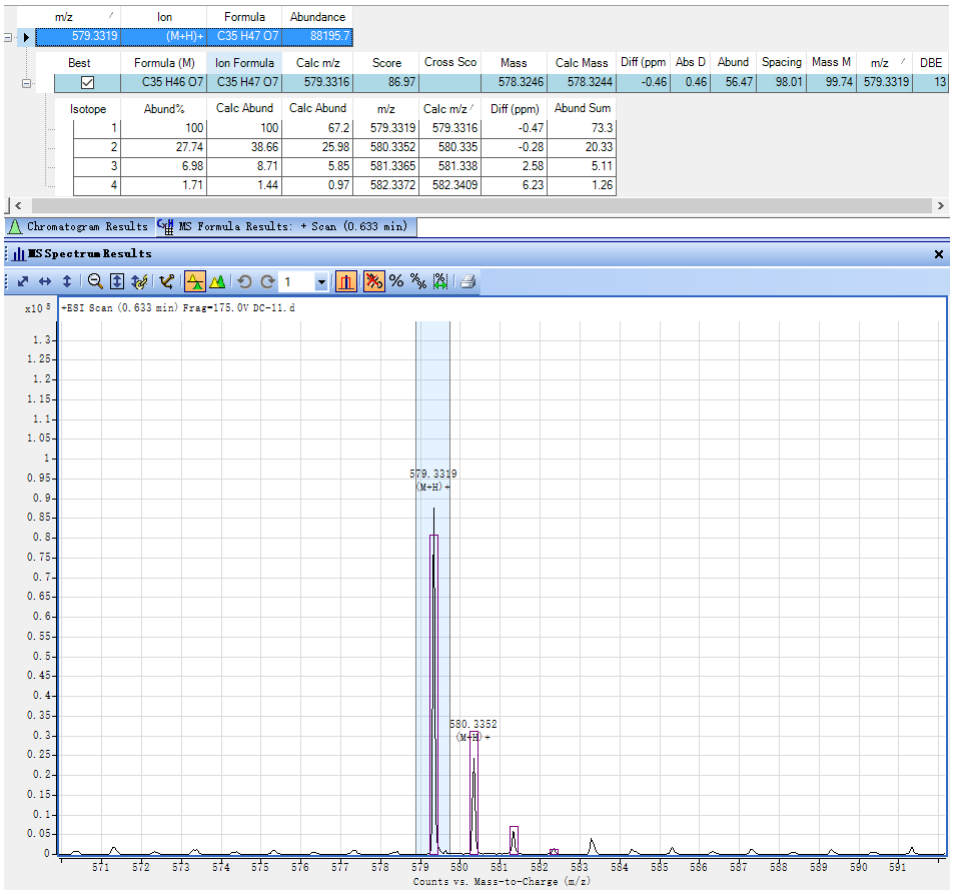

Figure S1. The HR-ESI-MS of compound 1

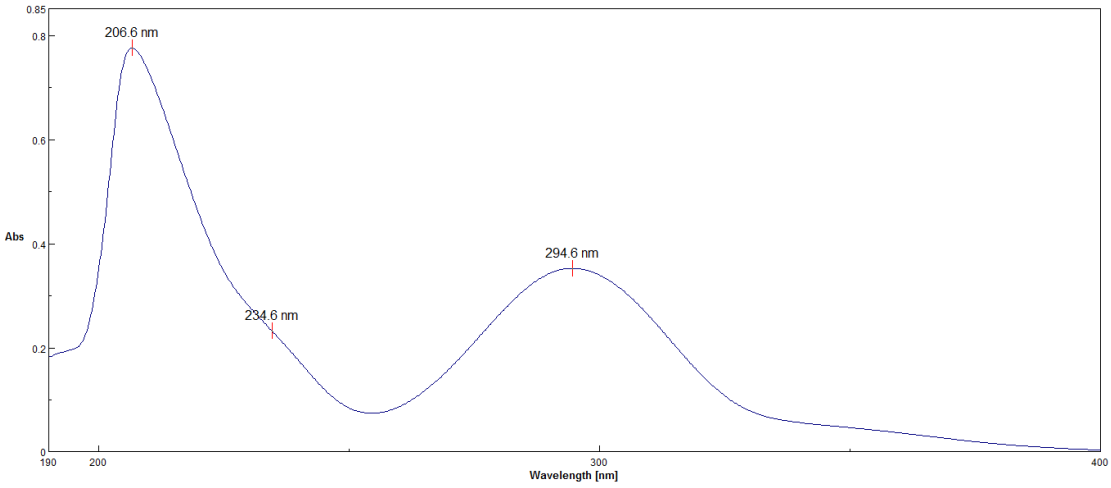

Figure S2. The UV of compound 1 in MeOH

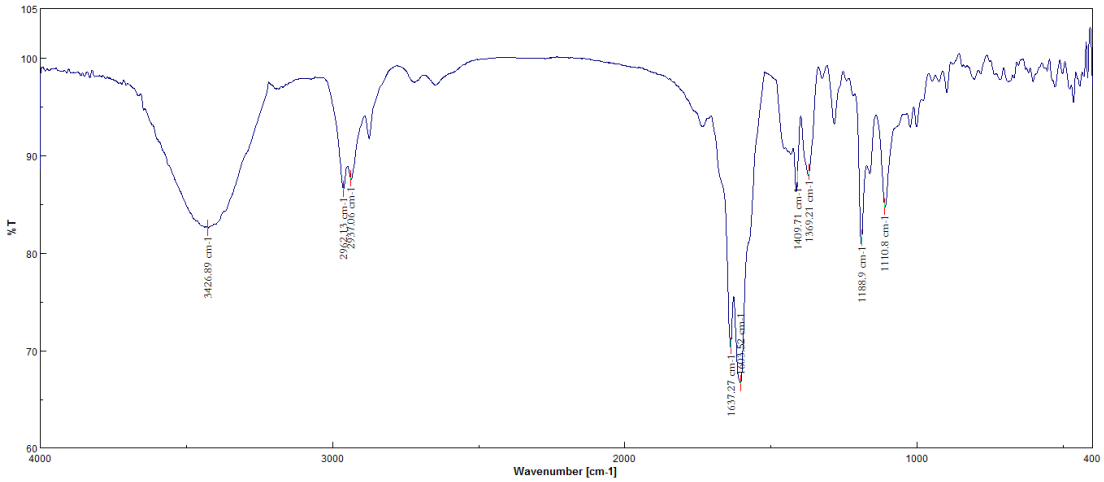

Figure S3. The IR (KBr disc) of compound 1

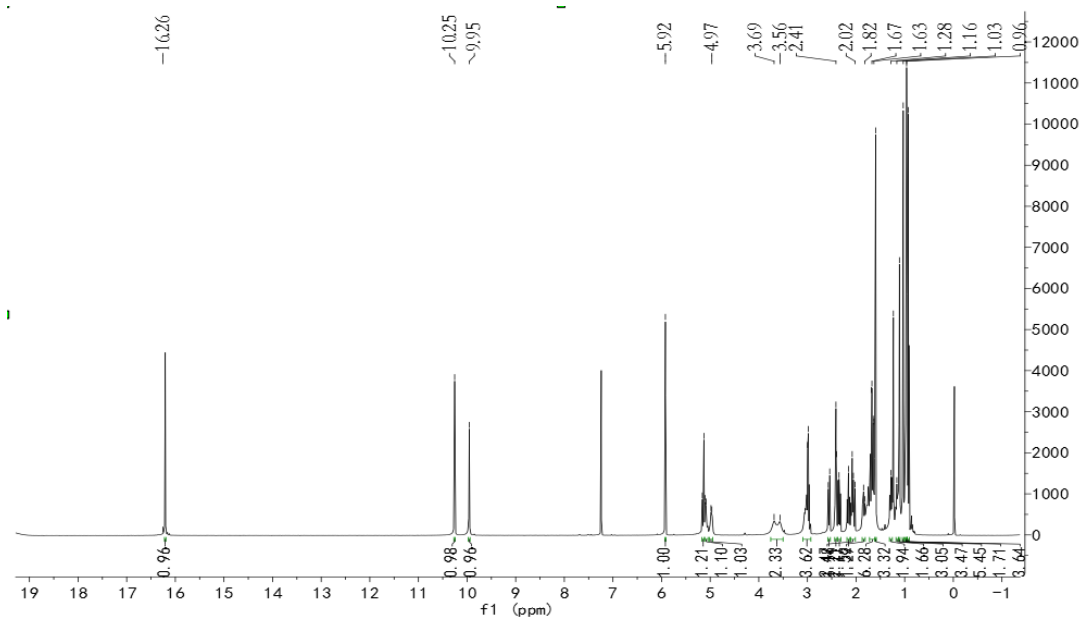

Figure S4. The ^{1}H NMR spectrum of compound 1 in $CDCl_3$

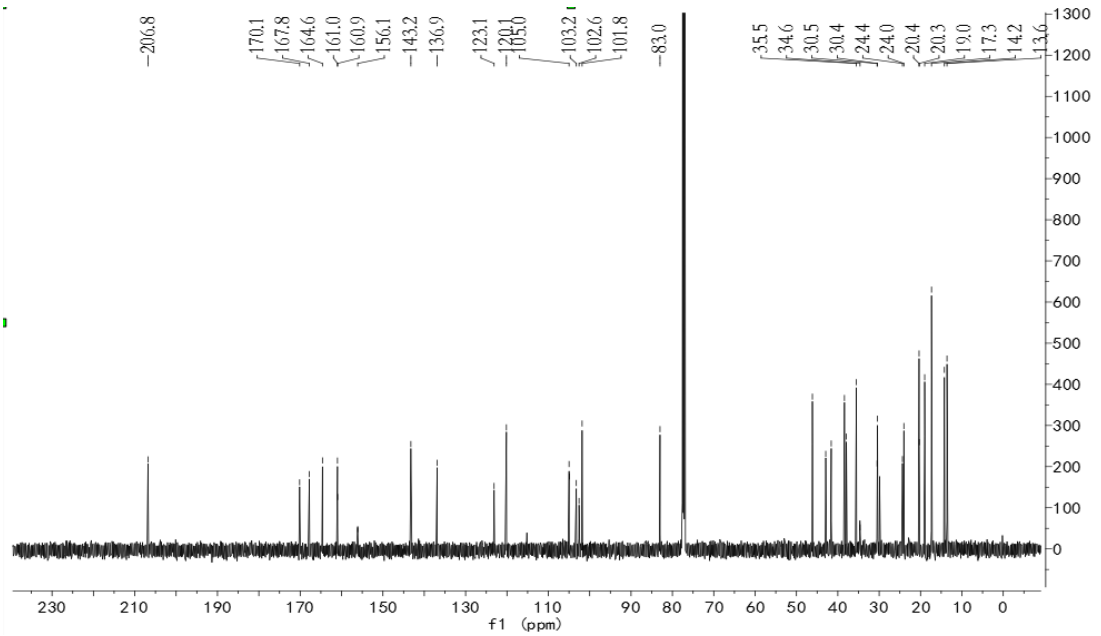

Figure S5. The ^{13}C NMR spectrum of compound 1 in $CDCl_3$

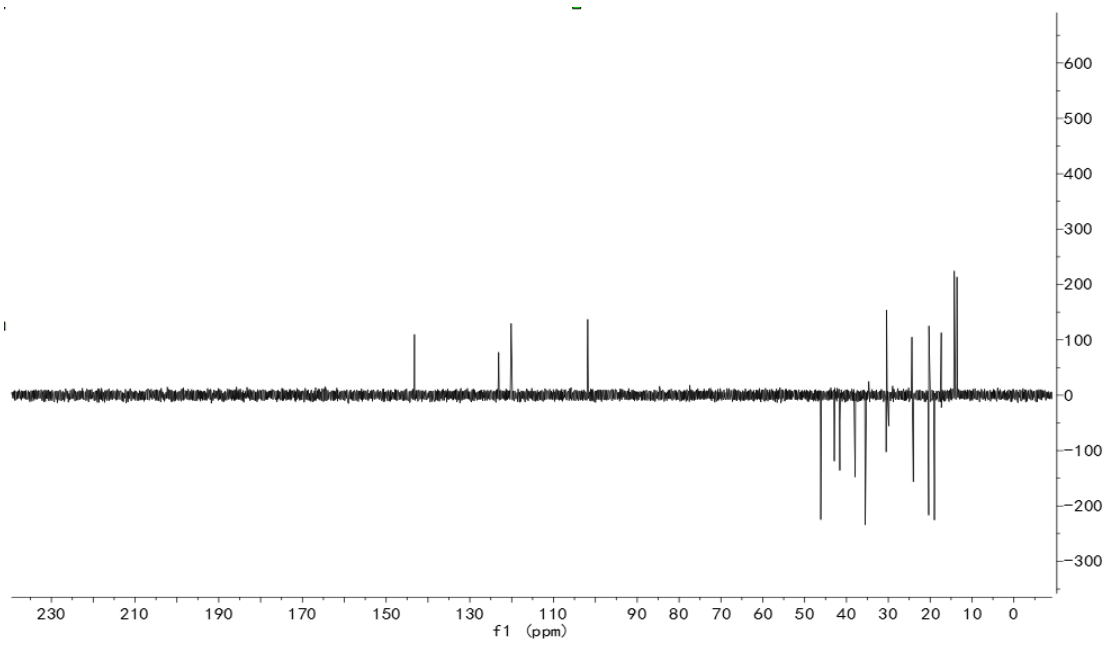

Figure S6. The DEPT-135 NMR spectrum of compound 1 in $CDCl_3$

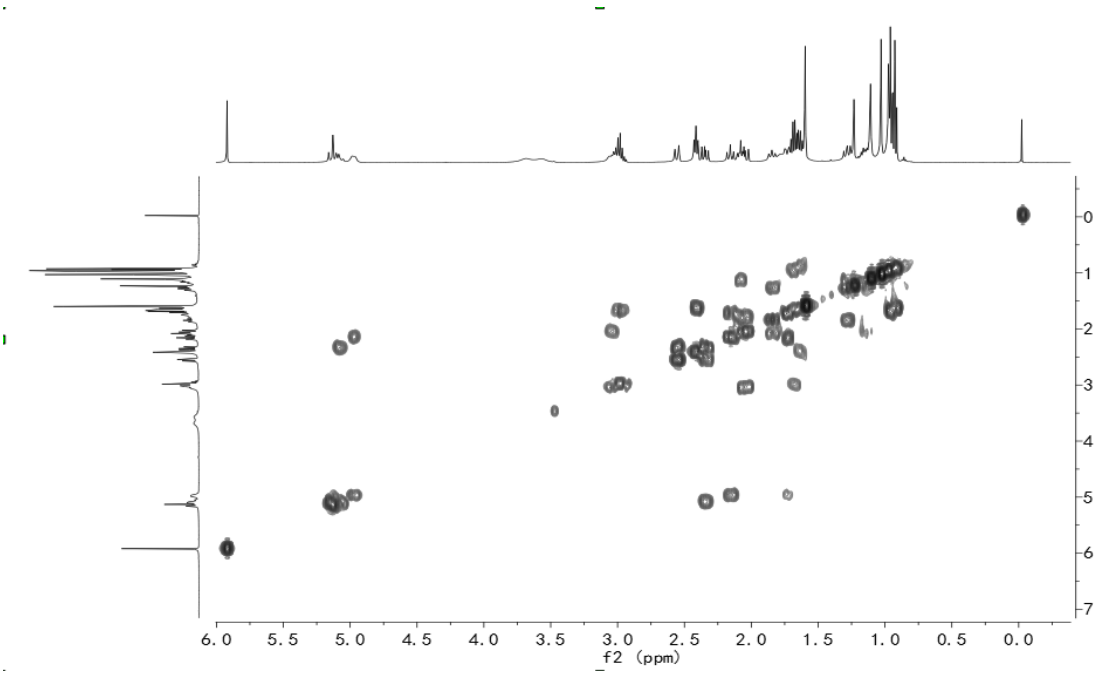

Figure S7. The ^{1}H-^{1}H COSY spectrum of compound 1 in $CDCl_3$

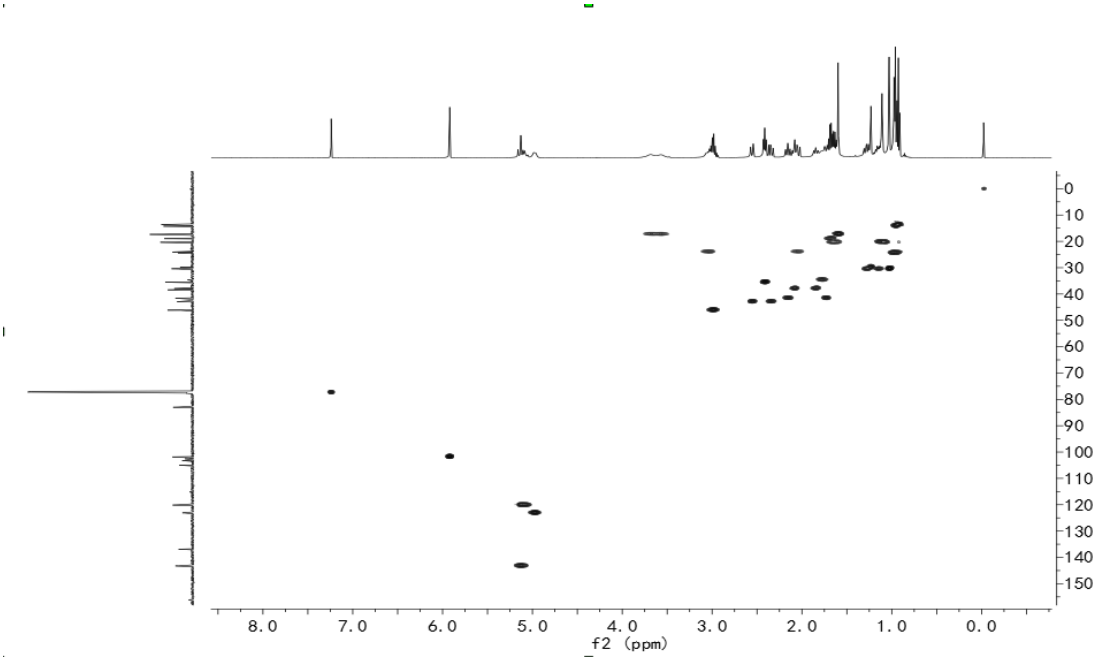

Figure S8. The HSQC spectrum of compound 1 in $CDCl_3$

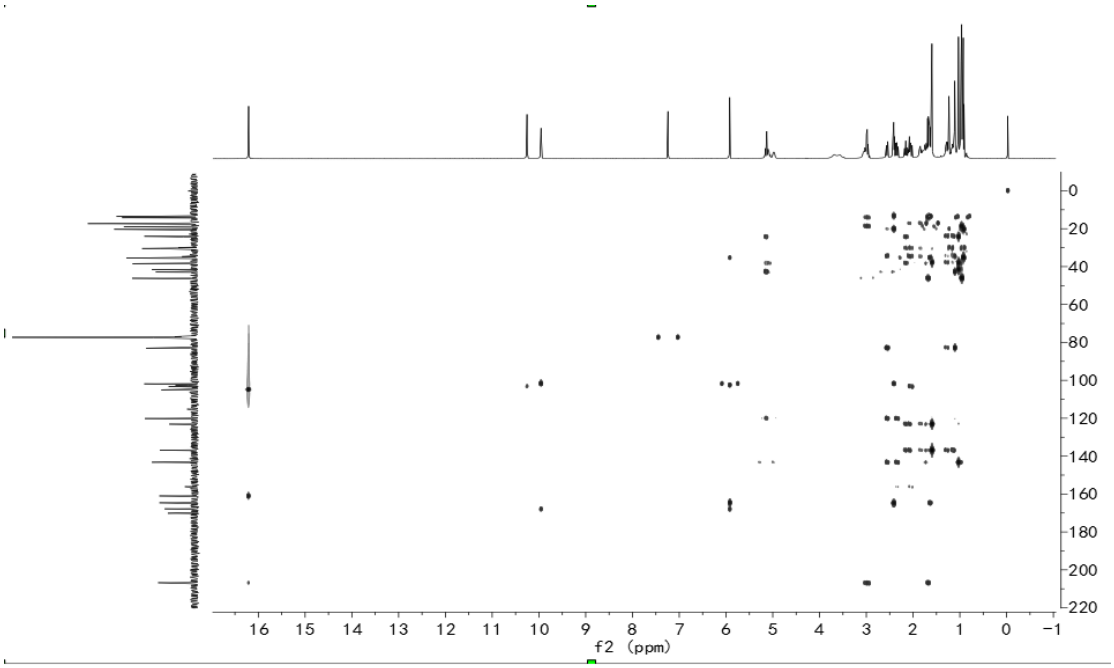

Figure S9. The HMBC spectrum of compound 1 in $CDCl_3$

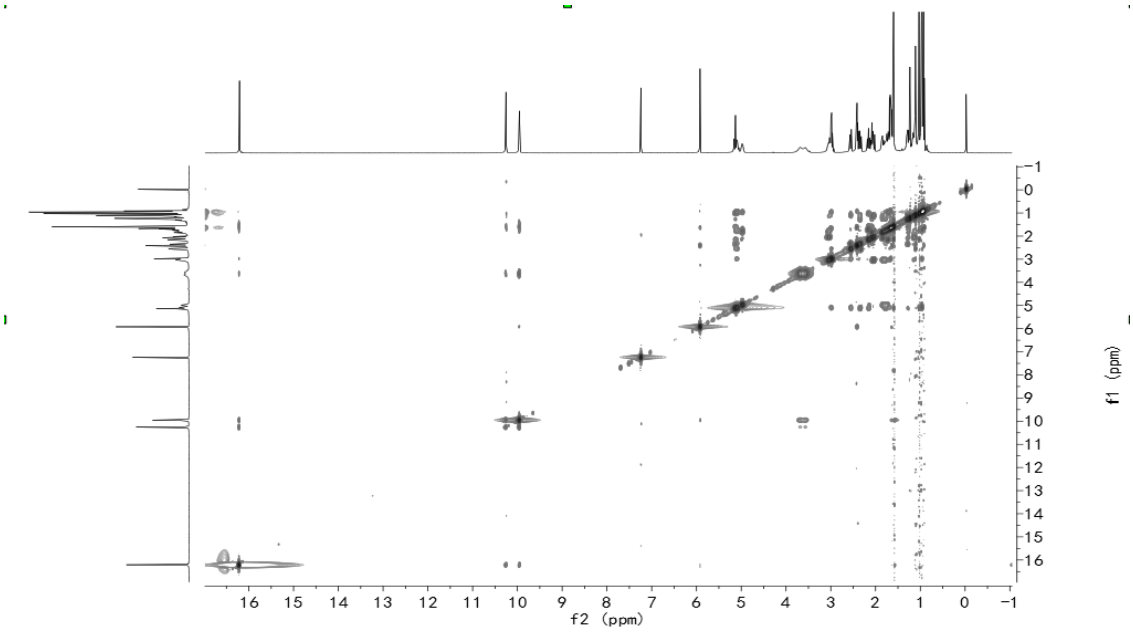

Figure S10. The NOESY spectrum of compound 1 in $CDCl_3$

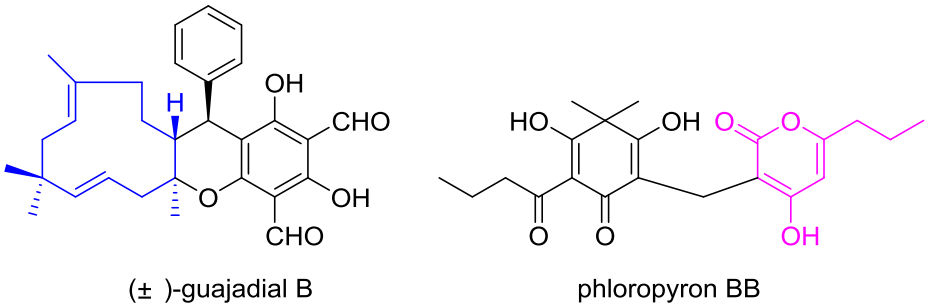

(±)-guajadial B　　phloropyron BB

Figure S11. The structures of (±)-guajadial B and phloropyron BB

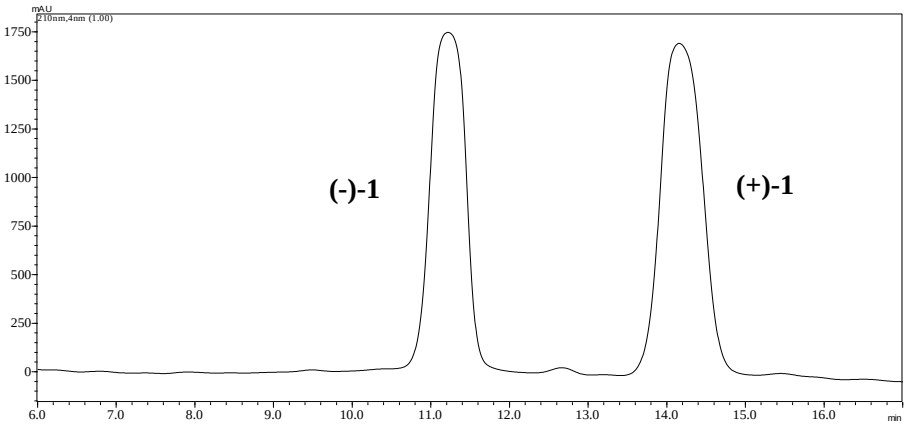

Figure S12. The chiral HPLC of compound 1

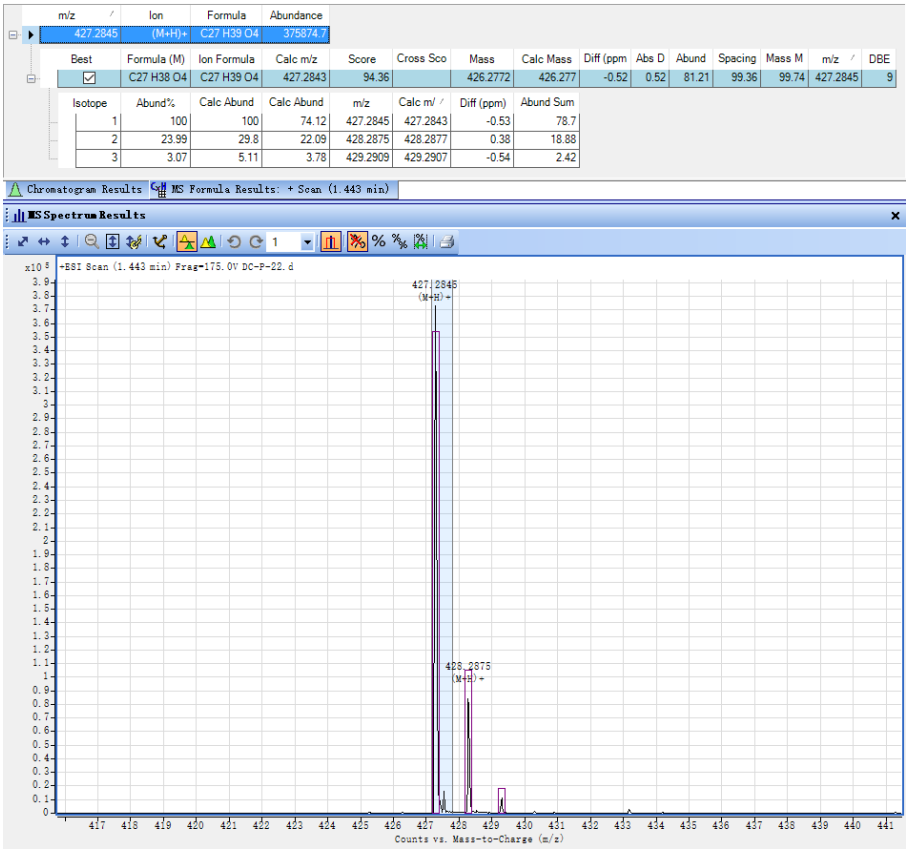

Figure S13. The HR-ESI-MS of compound 2

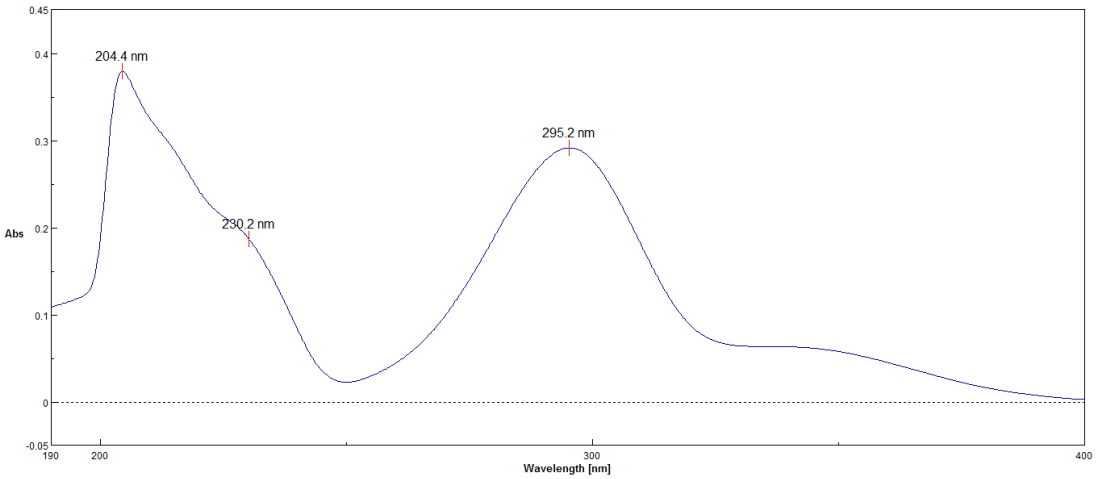

Figure S14. The UV of compound 2 in MeOH

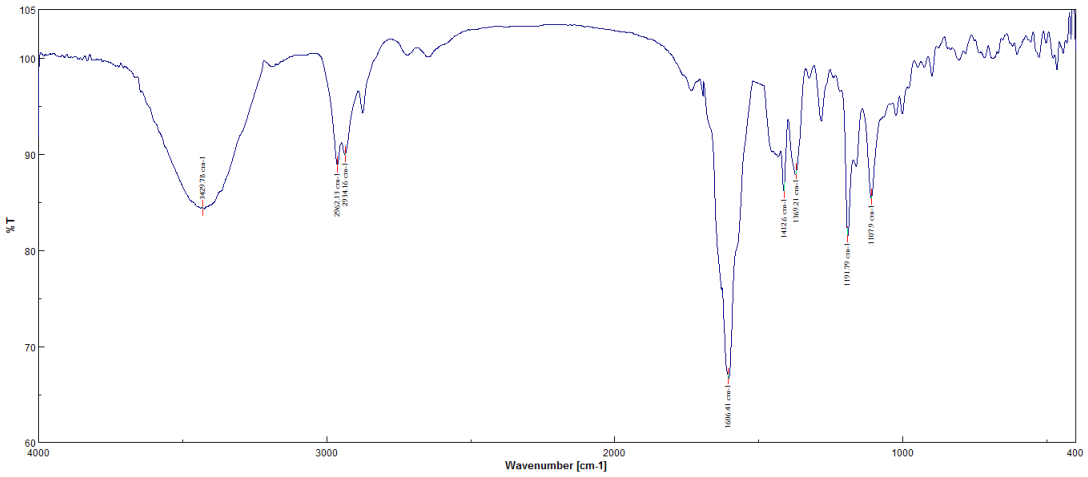

Figure S15. The IR (KBr disc) of compound 2

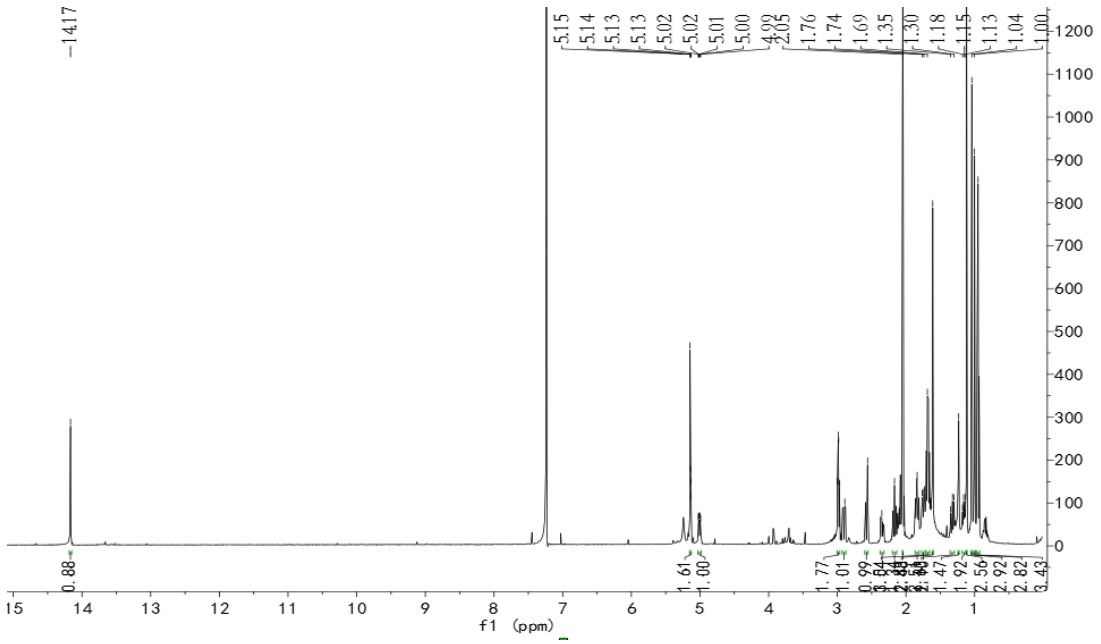

Figure S16. The ^{1}H NMR spectrum of compound 2 in $CDCl_3$

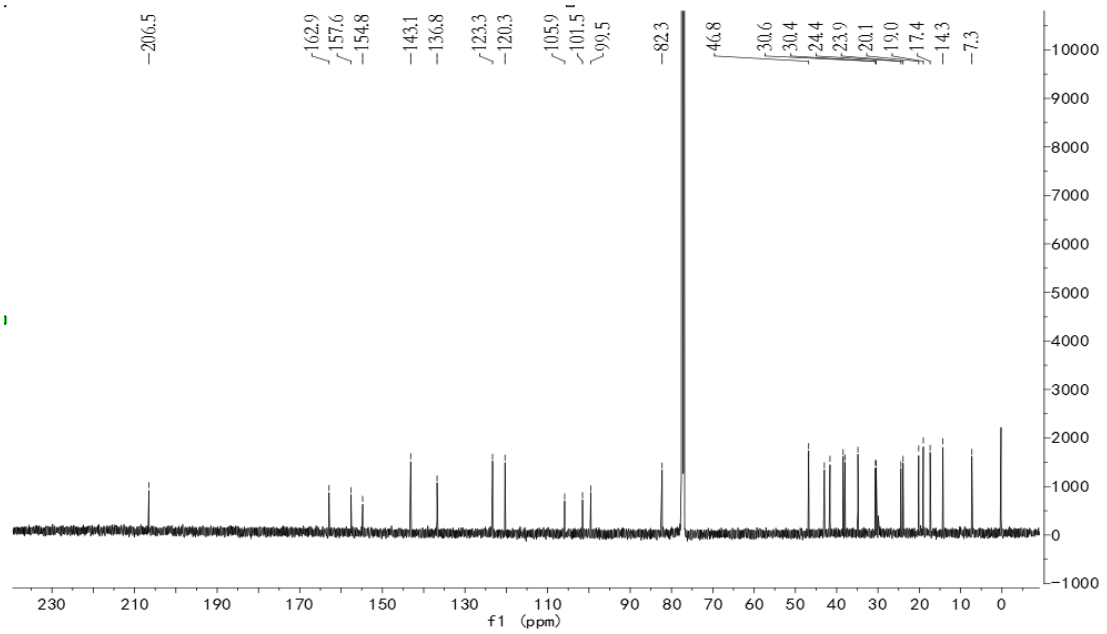

Figure S17. The ^{13}C NMR spectrum of compound 2 in $CDCl_3$

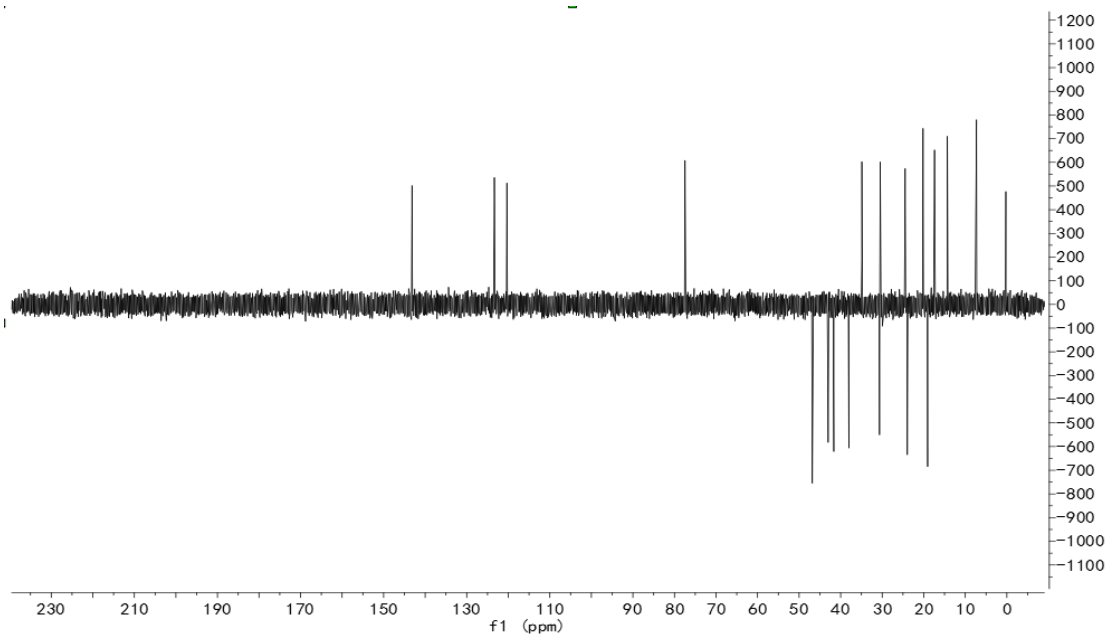

Figure S18. The DEPT-135 NMR spectrum of compound 2 in $CDCl_3$

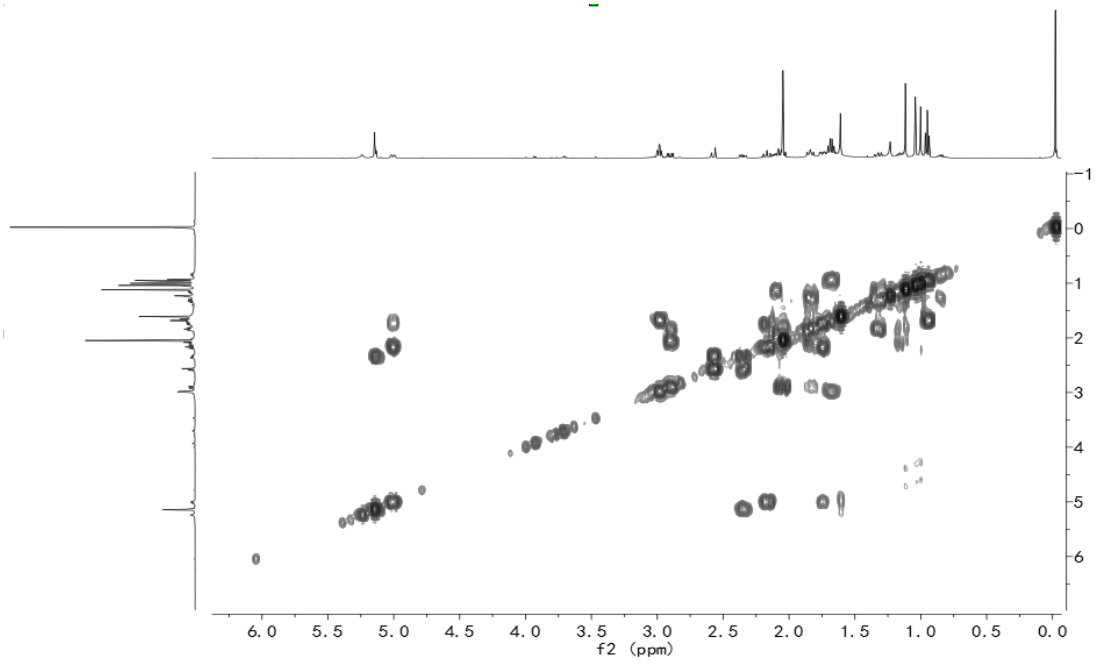

Figure S19. The ^{1}H-^{1}H COSY spectrum of compound 2 in $CDCl_3$

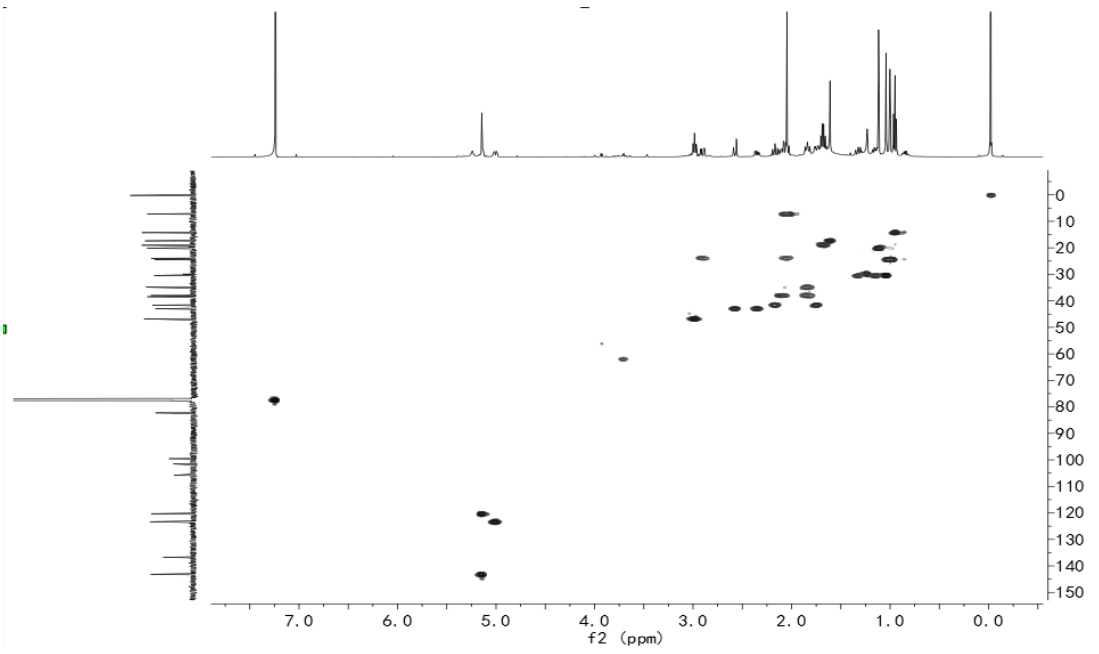

Figure S20. The HSQC NMR spectrum of compound 2 in $CDCl_3$

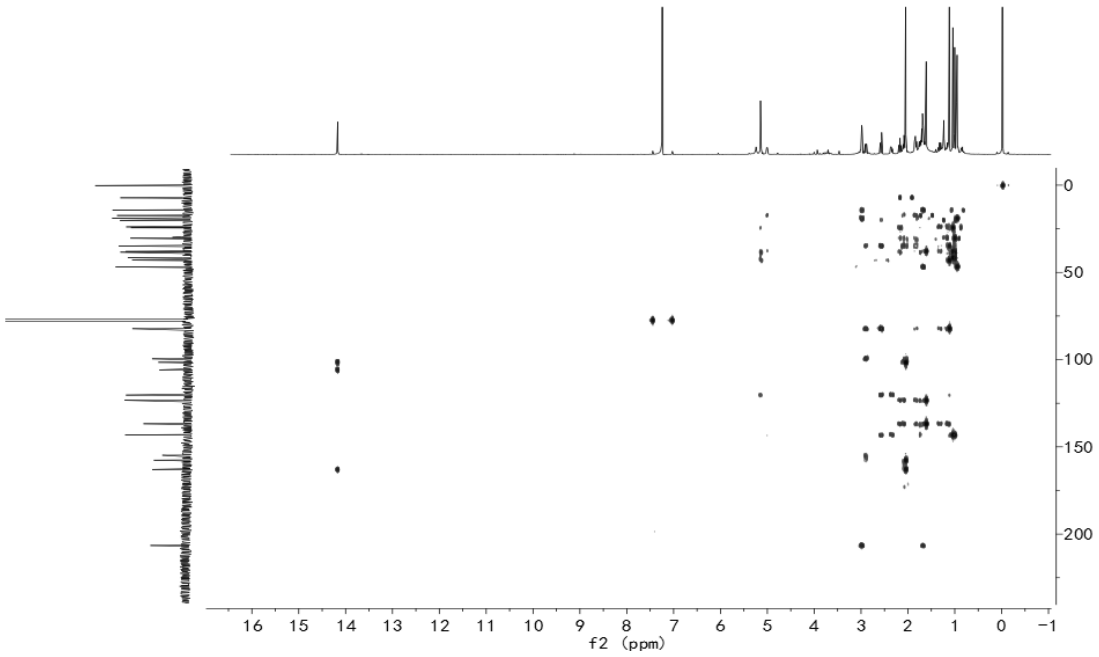

Figure S21. The HMBC spectrum of compound 2 in $CDCl_3$

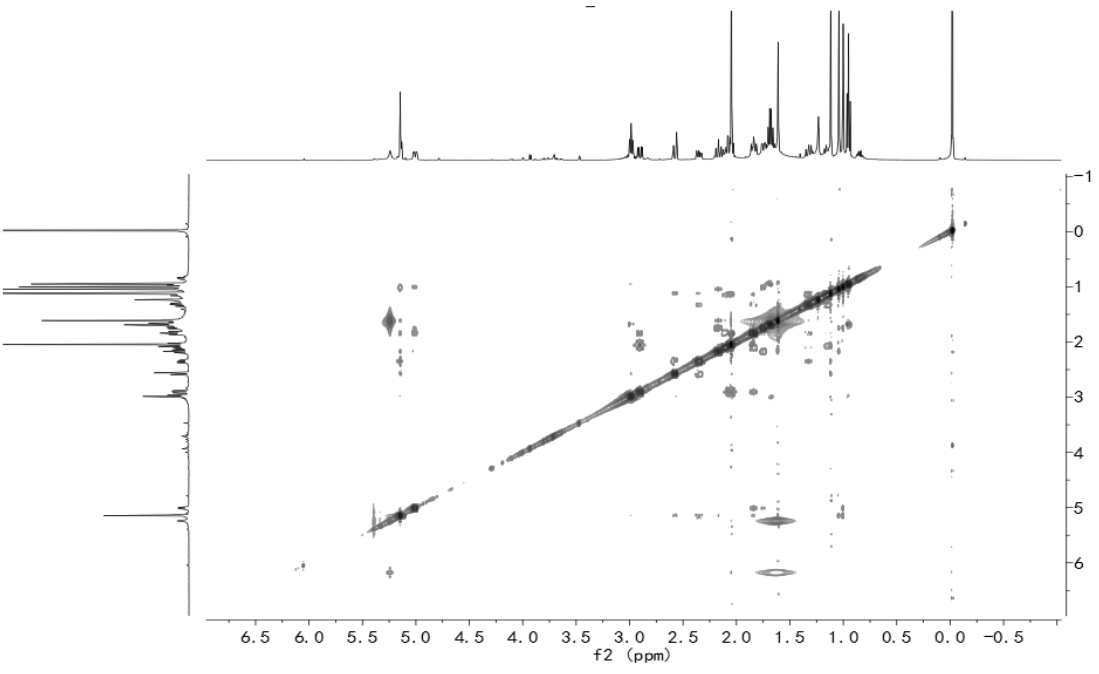

Figure S22. The NOESY spectrum of compound 2 in $CDCl_3$

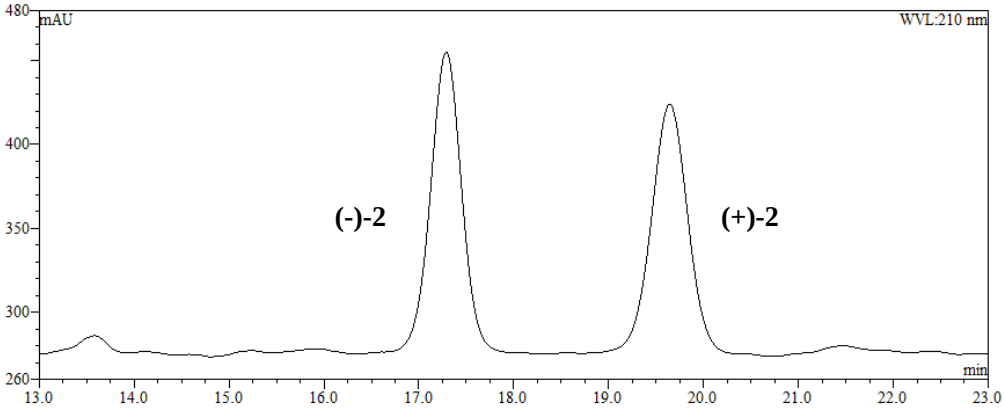

Figure S23. The chiral HPLC of compound 2

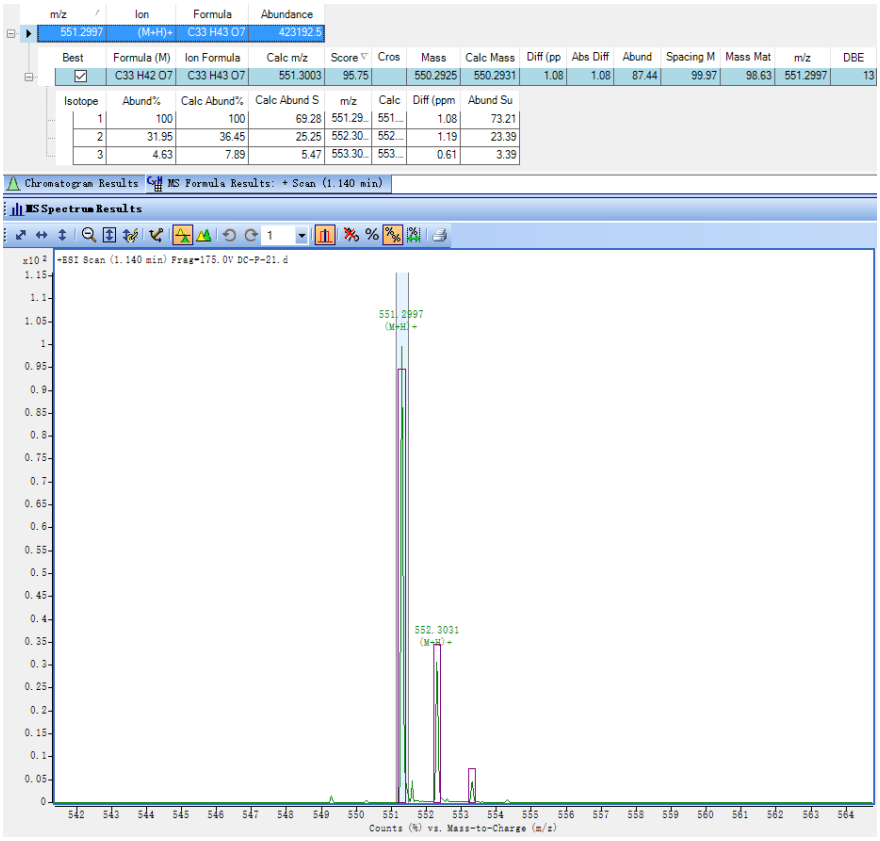

Figure S24. The HR-ESI-MS of compound 3

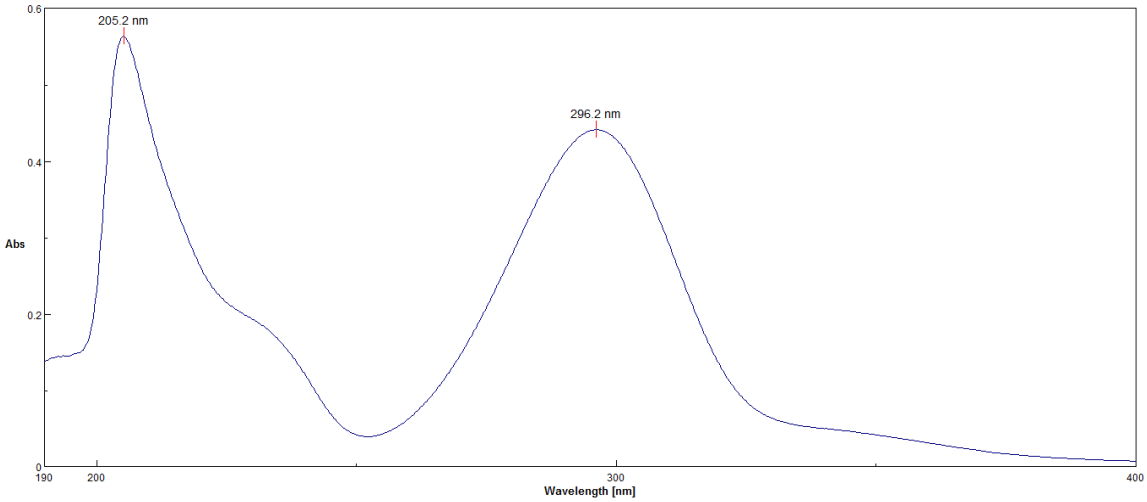

Figure S25. The UV of compound 3 in MeOH

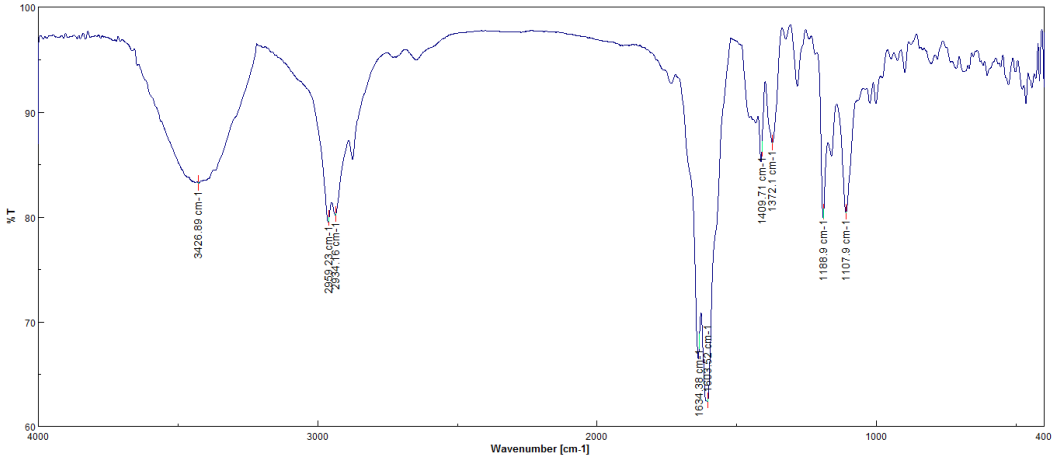

Figure S26. The IR (KBr disc) of compound 3 in MeOH

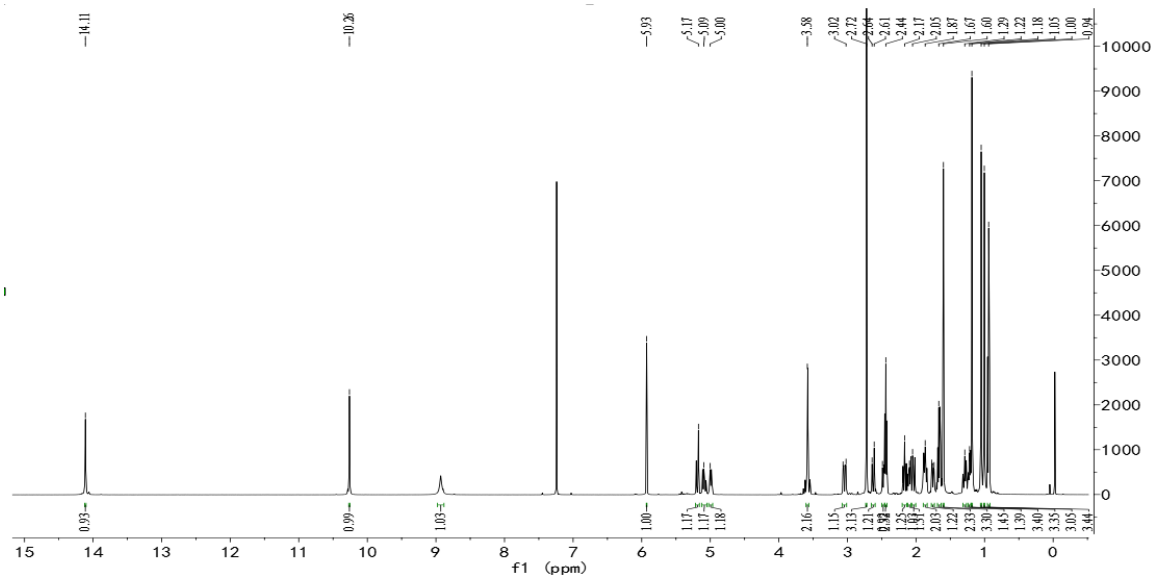

Figure S27. The ^{1}H NMR spectrum of compound 3 in $CDCl_3$

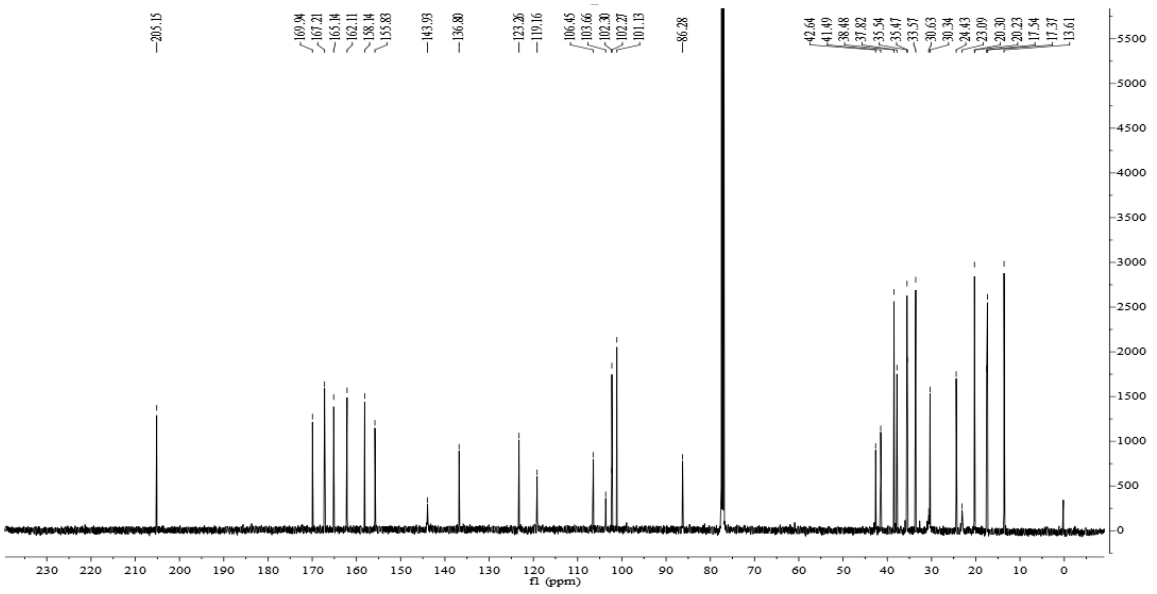

Figure S28. The ^{13}C NMR spectrum of compound 3 in $CDCl_3$

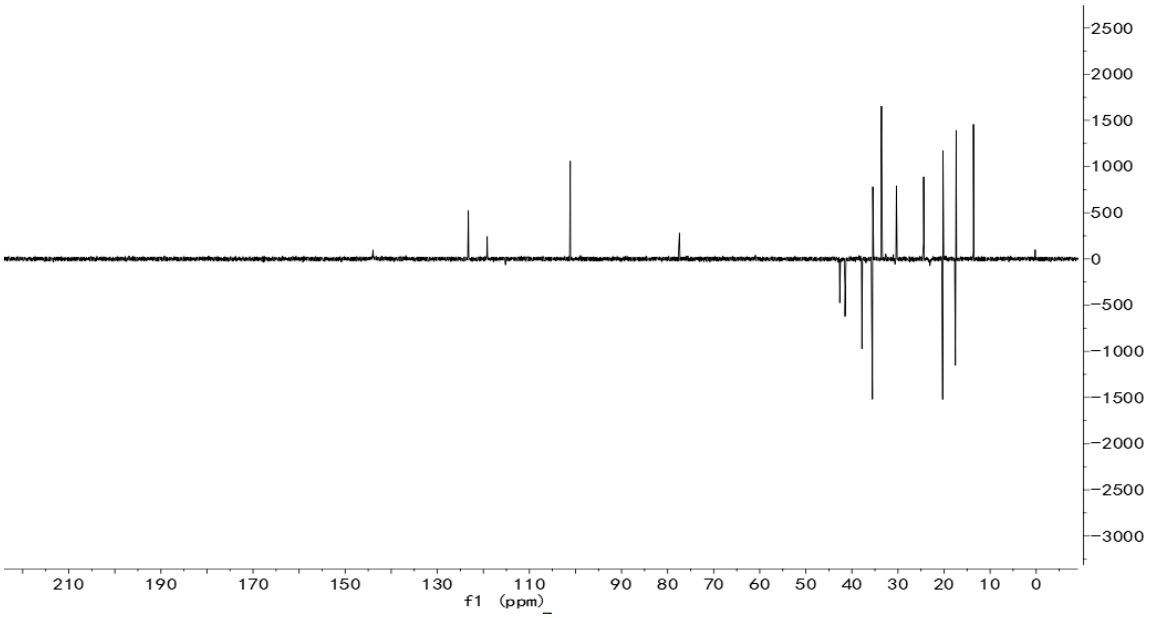

Figure S29. The DEPT-135 NMR spectrum of compound 3 in $CDCl_3$

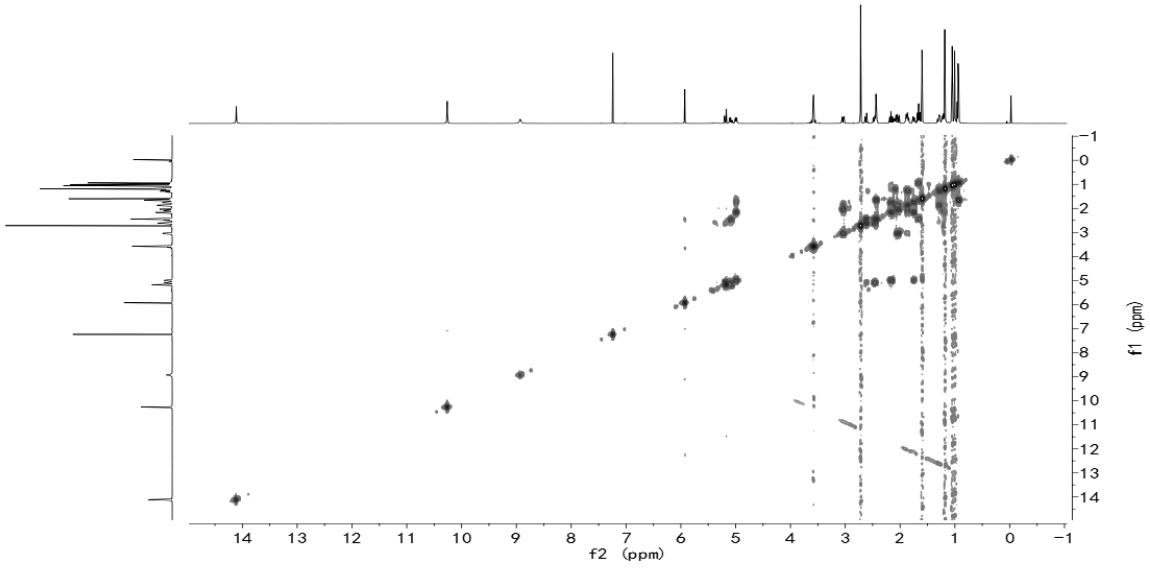

Figure S30. The ^{1}H-^{1}H COSY spectrum of compound 3 in $CDCl_3$

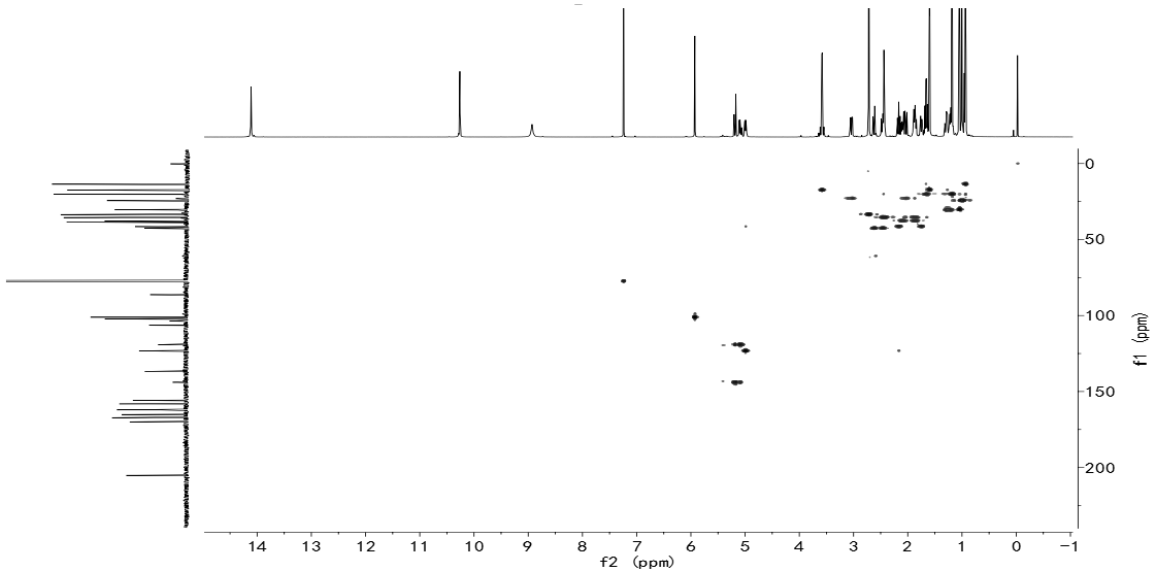

Figure S31. The HSQC spectrum of compound 3 in $CDCl_3$

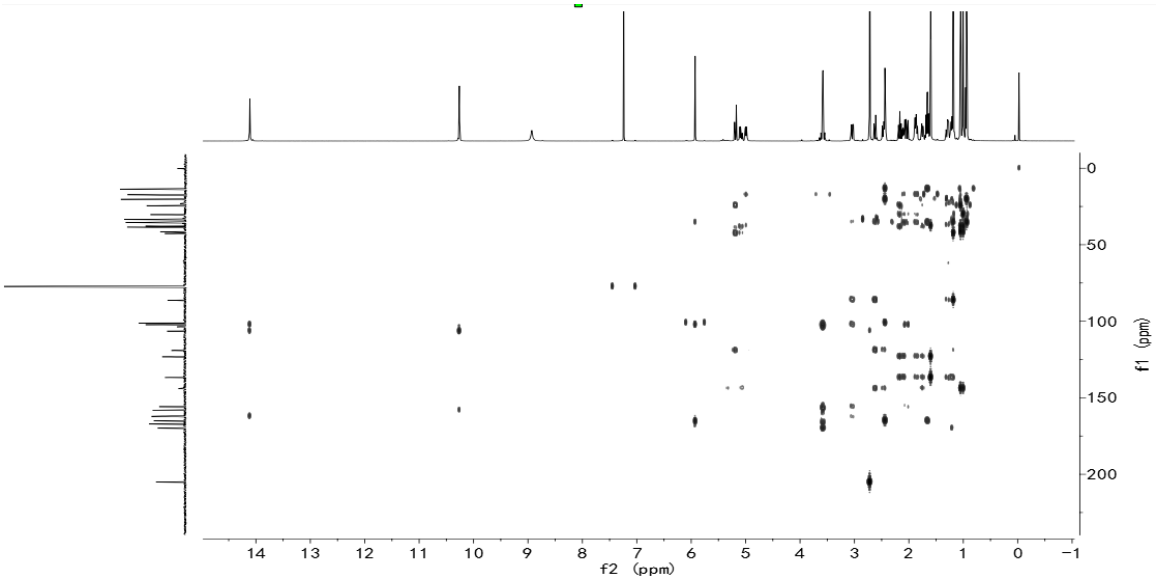

Figure S32. The HMBC spectrum of compound 3 in $CDCl_3$

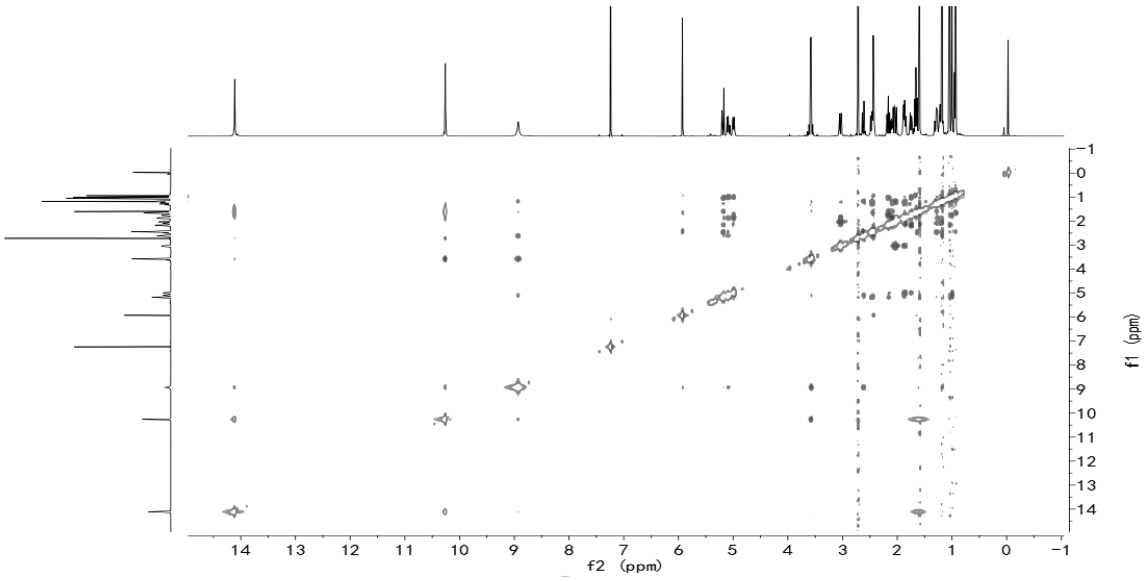

Figure S33. The NOESY spectrum of compound 3 in $CDCl_3$

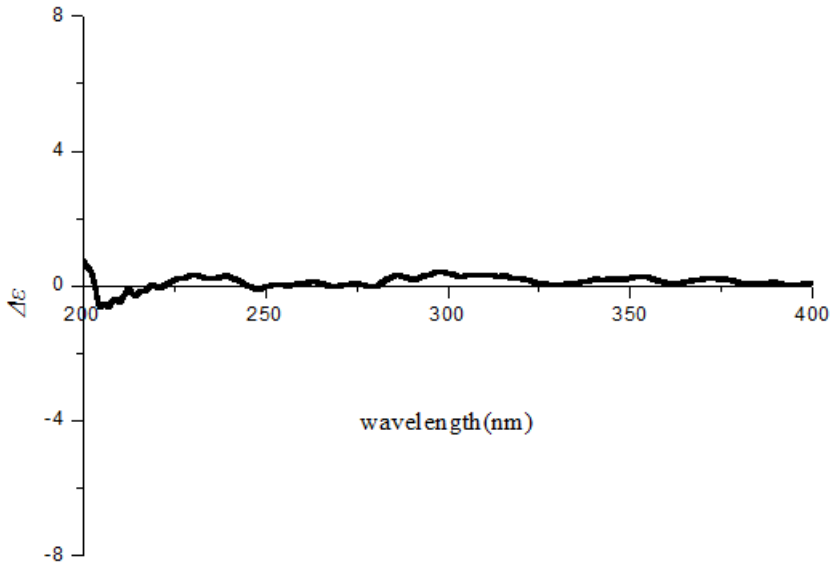

Figure S34. Experimental CD spectra of 3

Calculation details for compounds 1 and 2

The systematic random conformational analysis of the enantiomers of compound **1** & **2** was performed in the SYBYL 8.1 program by using MMFF94s molecular force field, which afforded 28 and 14 conformers for **1** and **2** respectively, with an energy cutoff of 10 kcal mol^{-1} to the global minima. All the obtained conformers were further optimized using DFT at the B3LYP/6-31+G(d) level in gas phase by using Gaussian09 software,[1] and 15 conformers of **1**, as well as 14 conformers of **2**, were selected. All of the optimized stable conformers were used for TDDFT computation of the excited stats at the same levels, with the consideration of the first 50 excitations. The overall ECD curves of **1** and **2** were weighted by Boltzmann distribution of each conformer (with a half-bandwidth of 0.25 eV), with a UV correction of 12 nm. The calculated ECD spectra of **1** and **2** were subsequently compared with the experimental one, respectively. The ECD spectra were produced by SpecDis 1.6 software.[2]

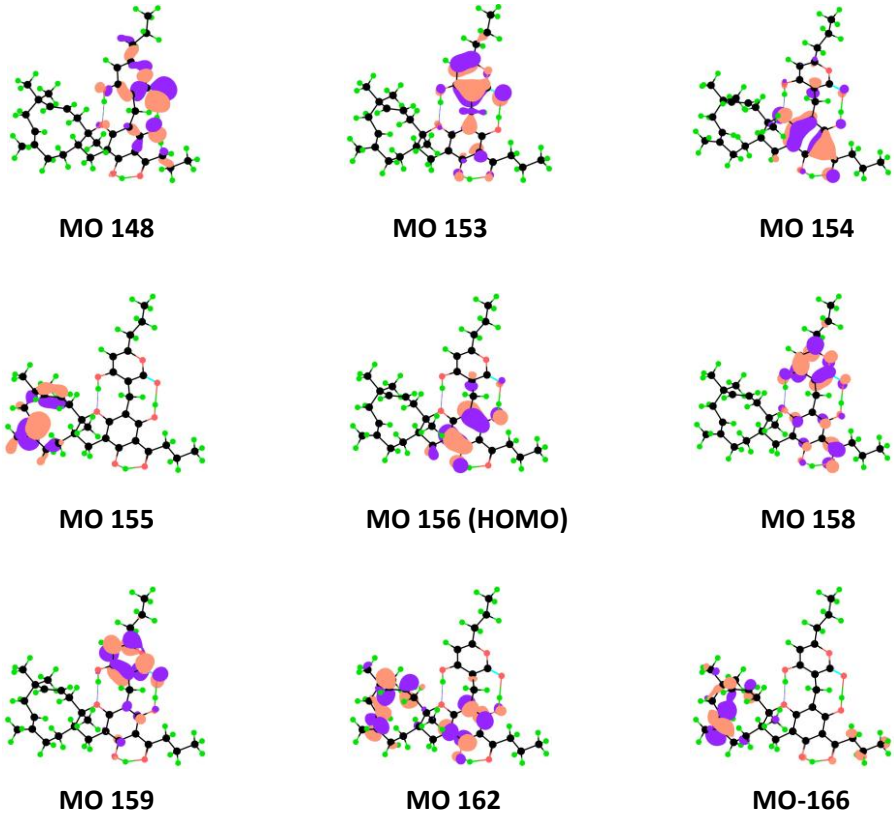

Figure S35 Key molecular orbitals involved in important transitions regarding the

ECD spectra of conformer 3 of **1** in the gas phase at the B3LYP/6-31+G(d) level.

Table S1 Key transitions and their related rotatory and oscillator strengths of conformer 3 of **1** at the B3LYP/6-31+G(d) level in the gas phase.

HOMO is 156

No.	Energy (cm^{-1})	Wavelength (nm)	R (length)	Osc. Strength	Major contribs
1	29548.33	338.4287	5.3267	0.0746	HOMO->LUMO (90%)
2	30809.79	324.5722	-9.4964	0.0166	HOMO->L+1 (91%)
3	34074.74	293.4725	-1.3994	0.0010	H-1->LUMO (99%)
4	34571.58	289.2549	8.974	0.0046	H-5->LUMO (55%), H-5->L+1 (25%)
5	34907.92	286.4680	-1.2213	0.0015	H-1->L+1 (92%)
6	35035.35	285.4260	-31.7213	0.0322	H-2->LUMO (60%), H-2->L+1 (27%)
7	35903.21	278.5266	-63.2945	0.1879	H-3->LUMO (13%), H-2->LUMO (20%), H-2->L+1 (57%)
8	36356.50	275.0540	82.452	0.4371	H-3->LUMO (78%), H-2->L+1 (12%)
9	37030.78	270.0456	-86.4976	0.1144	H-3->L+1 (95%)
10	38168.03	261.9994	-0.2112	0.0044	H-4->LUMO (95%)
11	38943.94	256.7793	-0.4721	0.0056	H-4->L+1 (95%)
12	40360.26	247.7685	-22.2686	0.0317	HOMO->L+2 (90%)
13	41250.70	242.4201	0.4089	0.0005	HOMO->L+3 (79%)
14	43448.58	230.1571	0.4892	0.0005	H-5->LUMO (31%), H-5->L+1 (68%)
15	43659.09	229.0474	18.7906	0.1124	HOMO->L+4 (66%)
16	44173.68	226.3792	3.8946	0.0350	H-2->L+2 (51%)
17	44573.73	224.3474	20.8158	0.0061	H-1->L+2 (23%), H-1->L+3 (35%), H-1->L+6 (18%)
18	44626.16	224.0838	-10.5969	0.0091	H-1->L+2 (64%)
19	44772.95	223.3491	-3.9825	0.0294	H-6->LUMO (16%), H-3->L+2 (15%), HOMO->L+5 (39%)
20	45077.83	221.8385	-24.4707	0.0175	H-8->LUMO (22%), H-8->L+1 (27%), HOMO->L+5 (16%)
21	45204.46	221.2171	-18.2941	0.0076	H-1->L+3 (24%), H-1->L+5 (27%)
22	45345.61	220.5285	3.2042	0.0569	H-8->L+1 (13%), H-6->L+1 (14%), H-3->L+2 (14%), HOMO->L+5 (15%)
23	45467.40	219.9378	12.4624	0.0035	H-2->L+3 (38%), H-2->L+4 (15%)
24	45665.81	218.9822	-0.5969	0.0016	HOMO->L+6 (63%), HOMO->L+9 (13%)
25	45720.66	218.7195	5.3183	0.0049	H-6->LUMO (12%), H-3->L+2 (12%), HOMO->L+7 (15%)
26	45877.13	217.9735	-7.741	0.0105	H-2->L+3 (15%), HOMO->L+7 (10%), HOMO->L+8 (52%)
27	46040.86	217.1984	5.45	0.0012	H-2->L+2 (17%), H-2->L+3 (15%), H-2->L+4 (12%), HOMO->L+7 (21%)
28	46439.31	215.3348	-39.9893	0.0558	H-6->LUMO (25%), H-1->L+6 (12%), HOMO->L+7 (21%)
29	46473.18	215.1779	17.1305	0.0093	H-1->L+6 (46%)
30	46590.13	214.6377	-58.5332	0.0491	H-6->LUMO (10%), H-3->L+3 (56%)
31	46861.14	213.3964	12.634	0.0087	H-1->L+4 (58%), H-1->L+5 (18%)
32	47120.04	212.2239	5.3538	0.0087	HOMO->L+6 (13%), HOMO->L+9 (67%)
33	47337.81	211.2476	4.4641	0.0033	H-1->L+7 (25%), H-1->L+8 (39%)
34	47446.70	210.7628	0.3312	0.0031	H-7->LUMO (48%), H-6->L+1 (42%)
35	47728.99	209.5163	6.6143	0.0418	H-1->L+5 (19%), H-1->L+7 (45%), H-1->L+8 (10%)

36	47845.95	209.0041	-7.973	0.0181	H-7->L+1 (24%), HOMO->L+10 (46%)
37	48007.26	208.3018	-2.1813	0.0228	H-7->L+1 (40%), HOMO->L+10 (25%)
38	48533.13	206.0448	12.2254	0.0085	H-4->L+2 (49%), H-2->L+4 (11%), H-2->L+5 (11%)
39	48579.92	205.8464	4.3534	0.0388	H-4->L+2 (15%), H-3->L+4 (12%), HOMO->L+12 (11%)
40	48616.21	205.6927	-0.3703	0.0920	H-4->L+2 (16%), H-3->L+4 (25%), H-2->L+5 (16%), HOMO->L+11 (13%)
41	48694.45	205.3622	-10.5135	0.0264	H-2->L+4 (21%), H-2->L+5 (24%), HOMO->L+11 (16%)
42	48954.97	204.2694	-2.7831	0.0023	H-8->LUMO (51%), H-8->L+1 (39%)
43	49103.37	203.6520	-0.0384	0.0023	H-4->L+3 (63%)
44	49211.45	203.2047	-0.172	0.0085	HOMO->L+12 (68%)
45	49568.76	201.7400	6.3293	0.0136	H-4->L+4 (19%), H-4->L+5 (18%), H-1->L+9 (15%)
46	49689.74	201.2488	40.1362	0.0238	H-2->L+6 (31%), H-2->L+7 (25%), H-2->L+9 (10%)
47	49747.81	201.0139	18.1082	0.0204	H-2->L+5 (10%), H-2->L+8 (22%), HOMO->L+13 (26%)
48	49838.15	200.6495	-9.5056	0.0093	H-2->L+6 (18%), H-2->L+7 (11%), HOMO->L+14 (36%)
49	50006.72	199.9731	7.7087	0.0356	H-2->L+8 (24%), HOMO->L+13 (30%)
50	50046.24	199.8152	121.9085	0.0358	H-2->L+8 (12%), H-1->L+9 (39%)

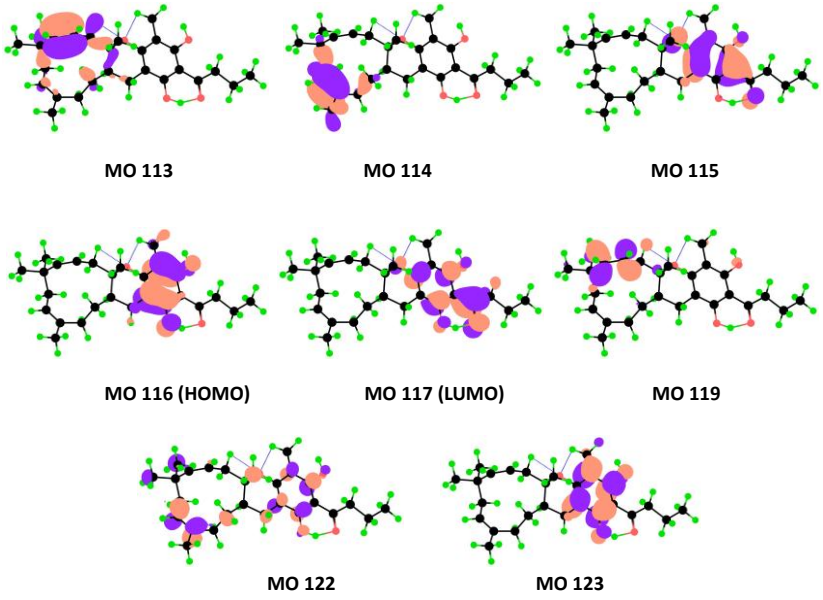

Figure S36 Key molecular orbitals involved in important transitions regarding the ECD spectra of conformer 3 of **2** in the gas phase at the B3LYP/6-31+G(d) level.

Table S2 Key transitions and their related rotatory and oscillator strengths of conformer 3 of **2** at the B3LYP/6-31+G(d) level in the gas phase.

HOMO is 116					
No.	**Energy (cm^{-1})**	**Wavelength (nm)**	**R (length)**	**Osc. Strength**	**Major contribs**
1	30975.13	322.8396	-1.5429	0.0453	HOMO->LUMO (96%)
2	34216.69	292.2550	-1.2406	0.0002	H-4->LUMO (97%)
3	36567.82	273.4645	-21.0525	0.4613	H-1->LUMO (95%)
4	37859.12	264.1371	0.0881	0.0036	H-2->LUMO (100%)

5	38668.91	258.6057	1.6879	0.0011	HOMO->L+1 (94%)
6	40634.49	246.0963	0.0988	0.0000	H-3->LUMO (100%)
7	42010.48	238.0358	-1.2188	0.0005	H-1->L+1 (95%)
8	42761.39	233.8558	-0.8040	0.0006	HOMO->L+2 (70%)
9	43473.58	230.0247	2.8749	0.0029	HOMO->L+2 (23%), HOMO->L+3 (52%),
10	44101.09	226.7518	0.0823	0.0001	HOMO->L+4 (79%)
11	44588.25	224.2743	18.4736	0.0065	H-2->L+1 (19%), H-2->L+2 (52%), H-2->L+3 (21%)
12	44695.52	223.7361	2.1246	0.0225	H-1->L+6 (42%), HOMO->L+5 (10%)
13	44862.48	222.9034	-1.9224	0.0200	HOMO->L+3 (15%), HOMO->L+5 (45%)
14	45285.12	220.8231	2.0253	0.0065	H-2->L+1 (32%), H-2->L+3 (52%)
15	45486.76	219.8442	4.0990	0.0032	H-1->L+2 (86%)
16	45586.77	219.3619	-33.7480	0.1880	H-5->LUMO (27%), HOMO->L+6 (48%)
17	46046.51	217.1717	14.9871	0.0657	H-5->LUMO (17%), HOMO->L+7 (44%)
18	46250.57	216.2136	-1.0875	0.0007	H-1->L+3 (25%), HOMO->L+7 (17%), HOMO->L+8 (26%)
19	46328.00	215.8522	2.3886	0.0022	H-1->L+3 (46%), HOMO->L+8 (18%)
20	46757.09	213.8713	-4.4553	0.0004	H-2->L+1 (26%), H-2->L+2 (17%), H-1->L+4 (16%)
21	46912.76	213.1616	0.4065	0.0026	H-1->L+4 (65%)
22	47303.13	211.4025	-11.0627	0.0018	H-2->L+4 (50%), H-2->L+5 (11%)
23	47569.30	210.2196	-3.1122	0.0081	H-1->L+5 (33%), HOMO->L+9 (23%)
24	47655.60	209.8389	9.9903	0.0177	H-3->L+1 (18%), HOMO->L+9 (31%)
25	47758.84	209.3853	4.2336	0.0109	H-3->L+1 (16%), H-1->L+5 (17%), HOMO->L+9 (23%)
26	48067.75	208.0397	-45.7951	0.2299	H-5->LUMO (43%), HOMO->L+6 (27%)
27	48325.04	206.9320	27.7250	0.0506	H-2->L+4 (18%), H-2->L+5 (44%)
28	48731.55	205.2059	-3.0746	0.0015	H-1->L+7 (64%)
29	48921.09	204.4108	2.6909	0.0045	HOMO->L+10 (74%)
30	49000.94	204.0777	-7.2700	0.0096	H-3->L+1 (33%), H-3->L+3 (26%)
31	49056.59	203.8462	0.4055	0.0004	H-1->L+5 (13%), H-1->L+8 (54%)
32	49275.17	202.9420	-27.8206	0.0341	H-2->L+6 (11%), H-2->L+7 (28%), HOMO->L+11 (13%)
33	49282.43	202.9121	22.8861	0.0364	H-2->L+7 (13%), HOMO->L+11 (43%), HOMO->L+12 (13%)
34	49613.93	201.5563	-2.6614	0.0022	HOMO->L+11 (19%), HOMO->L+12 (55%)
35	49813.15	200.7502	3.1713	0.0016	H-4->L+1 (67%), H-2->L+6 (16%)
36	49828.47	200.6885	-6.4020	0.0042	H-4->L+1 (21%), H-2->L+6 (50%), H-2->L+7 (16%)
37	50203.52	199.1892	-14.0958	0.0098	HOMO->L+13 (63%)
38	50276.11	198.9016	11.6479	0.0091	H-3->L+4 (25%), H-3->L+5 (28%)
39	50475.33	198.1166	6.6587	0.0025	H-3->L+2 (13%), H-3->L+4 (12%), H-1->L+9 (46%)
40	50503.56	198.0058	1.4977	0.0034	H-3->L+2 (15%), H-3->L+5 (25%), H-1->L+9 (28%)
41	50914.91	196.4061	5.7500	0.0157	HOMO->L+14 (52%), HOMO->L+15 (24%)
42	51066.54	195.8229	-0.6632	0.0002	H-4->L+5 (14%), H-4->L+6 (73%)
43	51114.93	195.6375	-38.2072	0.0125	H-6->LUMO (28%), HOMO->L+14 (19%), HOMO->L+15 (12%)
44	51198.82	195.3170	118.7148	0.0518	H-3->L+2 (26%), H-3->L+5 (12%), H-2->L+9 (11%)
45	51302.06	194.9240	28.6979	0.0551	H-6->LUMO (27%), HOMO->L+15 (32%), HOMO->L+16 (12%)
46	51548.86	193.9907	35.7010	0.1139	HOMO->L+16 (58%)
47	51671.46	193.5304	4.0121	0.0090	H-1->L+10 (62%)
48	51840.03	192.9011	30.6499	0.0751	H-3->L+7 (18%), H-2->L+8 (27%)

49	51859.39	192.8291	-18.3357	0.0341	H-1->L+10 (16%), H-1->L+11 (37%), H-1->L+12 (19%)
50	51987.63	192.3534	-0.7356	0.0076	H-2->L+8 (26%), H-2->L+9 (25%), H-2->L+10 (26%)

Reference

[1] Gaussian 09, Revision A.02, M. J. Frisch, G. W. Trucks, H. B. Schlegel, G. E. Scuseria, M. A. Robb, J. R. Cheeseman, G. Scalmani, V. Barone, B. Mennucci, G. A. Petersson, H. Nakatsuji, M. Caricato, X. Li, H. P. Hratchian, A. F. Izmaylov, J. Bloino, G. Zheng, J. L. Sonnenberg, M. Hada, M. Ehara, K. Toyota, R. Fukuda, J. Hasegawa, M. Ishida, T. Nakajima, Y. Honda, O. Kitao, H. Nakai, T. Vreven, J. A. Montgomery, Jr., J. E. Peralta, F. Ogliaro, M. Bearpark, J. J. Heyd, E. Brothers, K. N. Kudin, V. N. Staroverov, R. Kobayashi, J. Normand, K. Raghavachari, A. Rendell, J. C. Burant, S. S. Iyengar, J. Tomasi, M. Cossi, N. Rega, J. M. Millam, M. Klene, J. E. Knox, J. B. Cross, V. Bakken, C. Adamo, J. Jaramillo, R. Gomperts, R. E. Stratmann, O. Yazyev, A. J. Austin, R. Cammi, C. Pomelli, J. W. Ochterski, R. L. Martin, K. Morokuma, V. G. Zakrzewski, G. A. Voth, P. Salvador, J. J. Dannenberg, S. Dapprich, A. D. Daniels, O. Farkas, J. B. Foresman, J. V. Ortiz, J. Cioslowski, and D. J. Fox, Gaussian, Inc., Wallingford CT, 2009.

[2] T. Bruhn, A. Schaumlöffel, Y. Hemberger, G. Bringmann, SpecDis version 1.60, University of Wuerzburg, Germany, 2012.

LC-MS and GC-MS analyses of the petroleum ether part extract of *D. championii*.

LC-MS conditions: LC-MS analysis was performed on a HPLC system coupled with a LC/MSD TOF mass spectrometer and an ESI source in positive mode. All the separations were carried out at 25 ℃ on a RP-18 column (5 μm, 4.6 mm × 250 mm) using a gradient program with the mobile phase CH_3CN/H_2O/HCOOH (70:30:0.1 to 95:5:0.1, *v*/*v*/*v*) as eluent. The conditions of MS analysis were as follows: drying gas (N_2) flow-rate, 11 L/min; drying gas temperature, 325 ℃; nebulizing gas (N_2) pressure, 35 psi; capillary voltage, 3000 V; fragmentor, 100 V.

GC-MS conditions: GC-MS analysis was performed on a GC-MS system coupled with a quadrupole mass spectrometer and an EI source. Chromatographic resolution was achieved with a GC column (0.25 μm, 0.25 mm × 30 m). The oven was maintained at the initial temperature of 75 ℃ for one minute, then heated to 280 ℃ at the rate of 10 ℃ min^{-1} with a hold of three minutes, and finally ramped to 310 ℃ at 30 ℃ min^{-1}. Helium gas was used as the carrier gas at a flow of 1.2 mL min^{-1}. The ion source was 280 ℃ and the electron impact ionization energy was 70 eV. Mass spectra scan range was set at *m/z* 50-600.

Result: In order to provide more supporting evidences for the speculative biosynthetic scheme in the manuscript, the detection of the proposed precursors was carried out with the LC-MS and GC-MS. The exact mass of the precursors were presented in the extracted-ion chromatogram (EIC) for the petroleum ether part extract of the *D. championii* as follow. The above results indicated that the speculative biosynthetic pathway was logical.

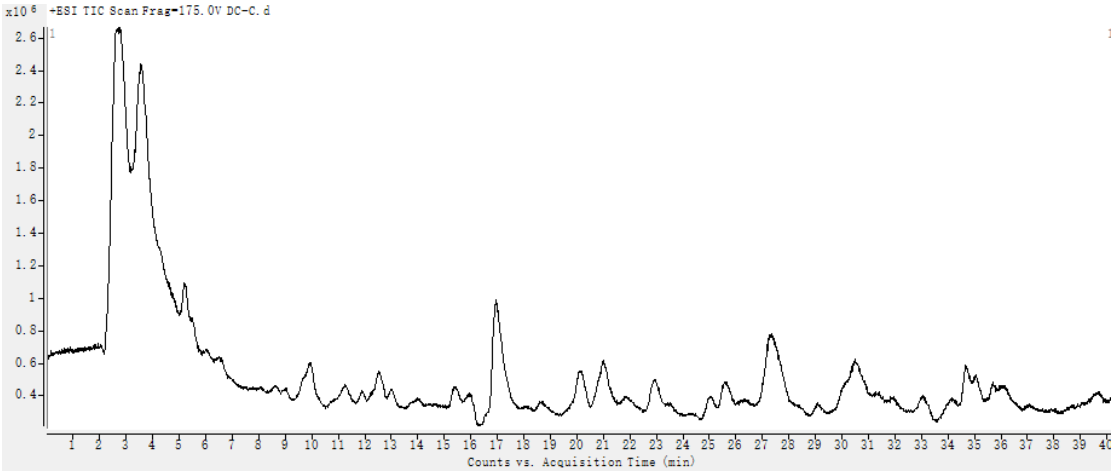

Figure S37. The total ion chromatogram (TIC) for the petroleum ether part extract of *D. championii* with the mobile phase $CH_3CN/H_2O/HCOOH$ (70:30:1 to 95:5:1, *v*/*v*/*v*) used as eluent

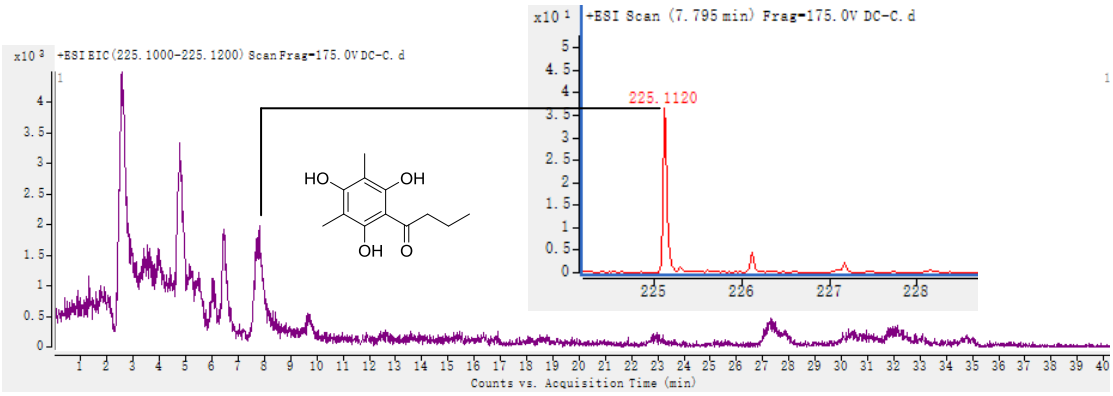

Figure S38. The extracted-ion chromatogram (EIC) for *m/z* 225.1000-225.1200 (calcd for $C_{12}H_{17}O_4$: *m/z* 225.1121), retention time: 7.795 min; *m/z* 225.1120 $[M + H]^+$

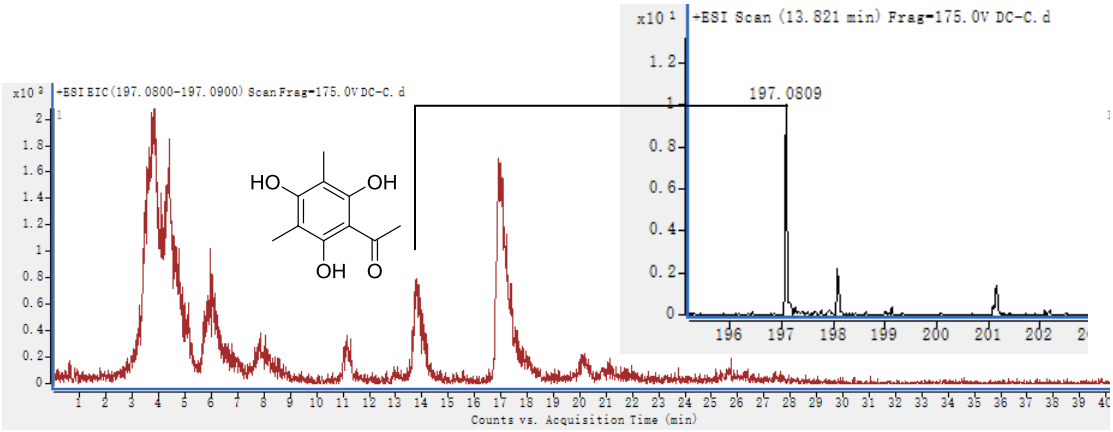

Figure S39. The extracted-ion chromatogram (EIC) for *m/z* 197.0800-197.0900 (calcd for $C_{10}H_{13}O_4$: *m/z* 197.0808), retention time: 13.821 min; *m/z* 197.0809 [M + H]$^+$

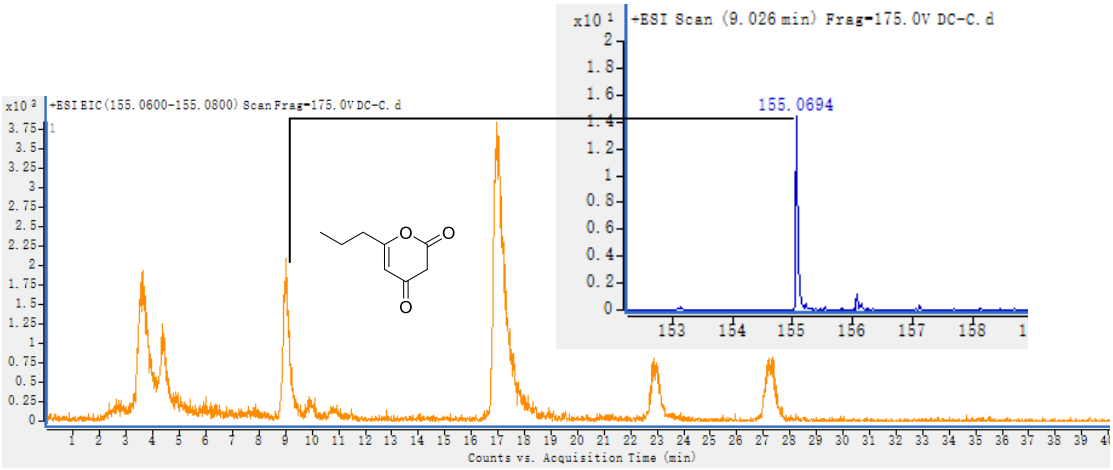

Figure S40. The extracted-ion chromatogram (EIC) for *m/z* 155.0600-155.0800 (calcd for $C_8H_{11}O_3$: *m/z* 155.0703), retention time: 4.778 min; *m/z* 155.0694 [M + H]$^+$

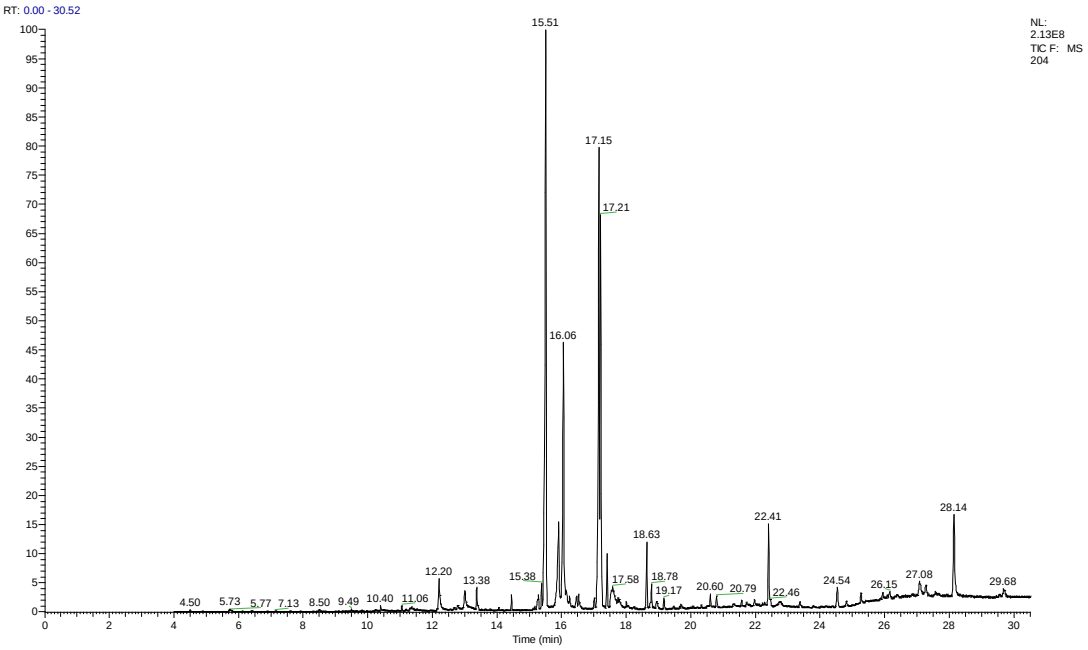

Figure S41. The total ion chromatogram (TIC) for the petroleum ether part extract of *D. championii*

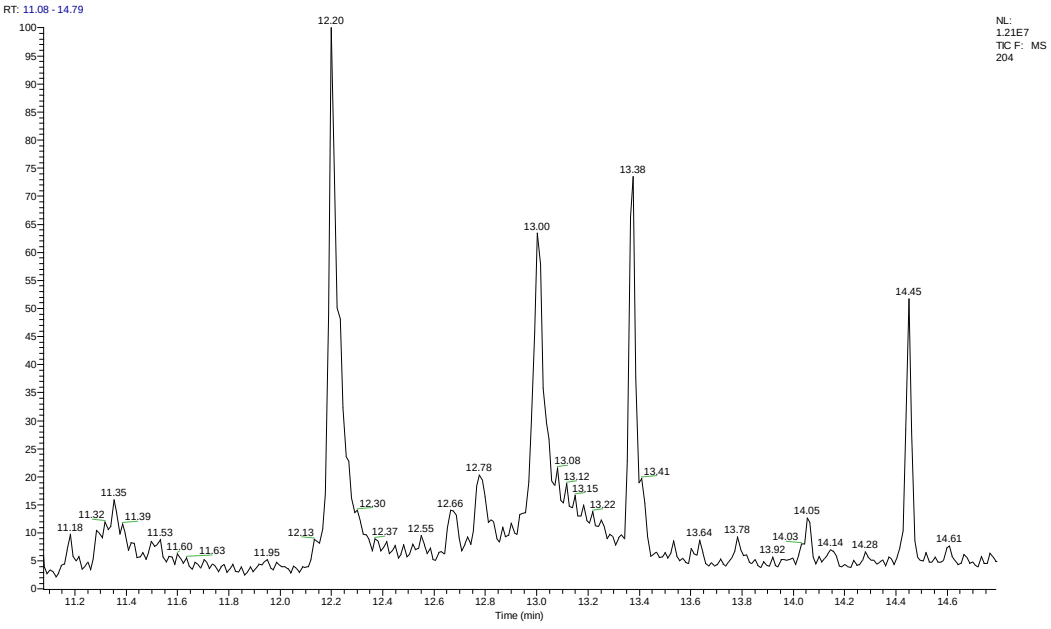

Figure S42. The extracted-ion chromatogram (EIC) for *m/z* 204

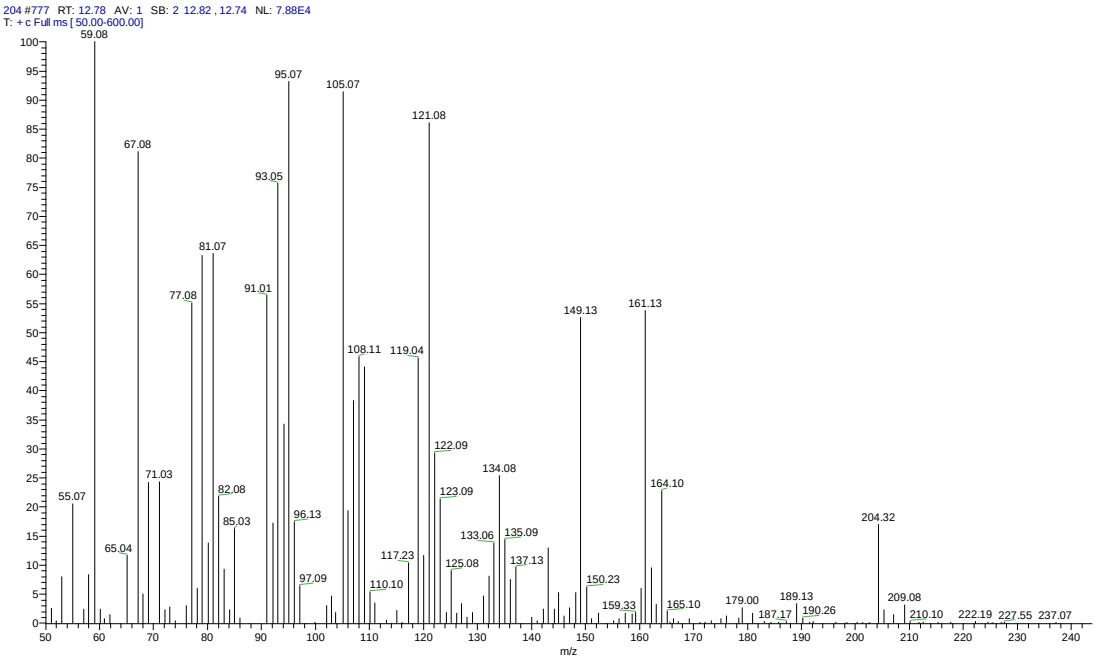

Figure S43. The enlarged extracted-ion chromatogram (EIC) for *m/z* 204 at the retention time of 12.78 min

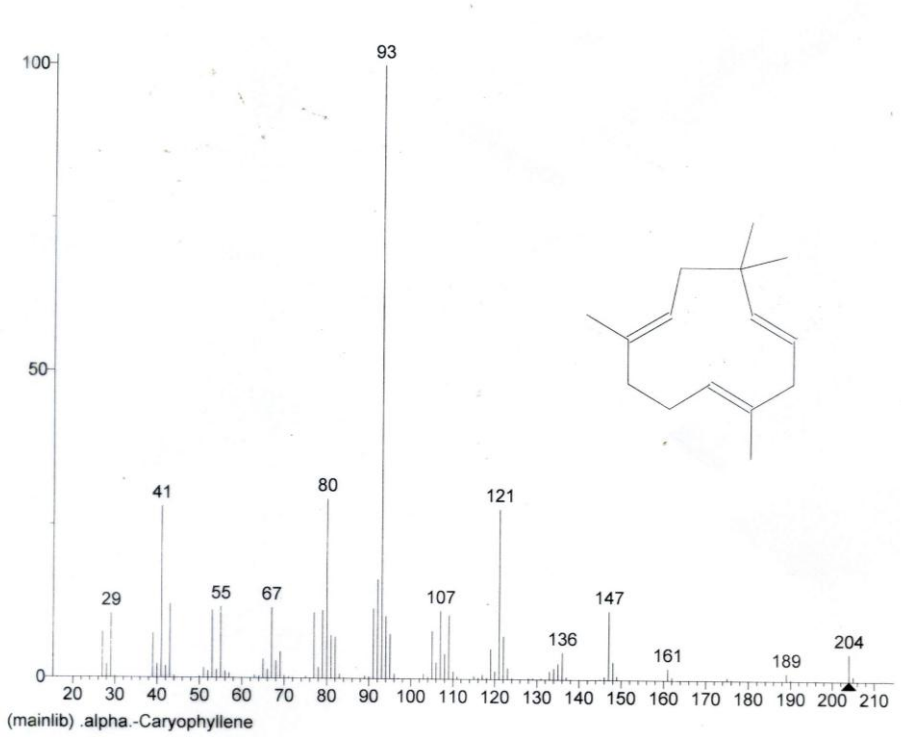

Figure S44. The reference of the extracted-ion chromatogram (EIC) for humulene searched in the NIST04 spectra library